Molecular basis of USP7 inhibition by selective small molecule inhibitors

Andrew P. Turnbull[1*#], Stephanos Ioannidis[2*#%], Wojciech W. Krajewski[1*], Adan Pinto-Fernandez[3], Claire Heride[5], Agnes C.L. Martin[4], Louise M. Tonkin[4], Elizabeth C. Townsend[2], Shane M. Buker[2$], David R. Lancia Jr.[2], Justin A. Caravella[2], Angela V. Toms[2], Thomas M. Charlton[3$], Johanna Lahdenranta[2], Erik Wilker[2], Bruce C. Follows[2], Nicola J. Evans[1$], Lucy Stead[5], Cristina Alli[4], Vladislav V. Zarayskiy[2], Adam C. Talbot[2], Alexandre J. Buckmelter[2], Minghua Wang[2], Crystal L. McKinnon[2], Fabienne Saab[1], Joanna F. McGouran[3$], Hannah Century[3$], Malte Gersch[6], Marc S. Pittman[1$], C. Gary Marshall[2], Tony M. Raynham[1$], Mary Simcox[2$], Lorna M.D. Stewart[1], Sheila B. McLoughlin[4], Jaime A. Escobedo[2], Kenneth W. Bair[2$], Christopher J. Dinsmore[2%], Tim R. Hammonds[1%], Sunkyu Kim[2%], Sylvie Urbé[5%], Michael J. Clague[5%], Benedikt M. Kessler[3#%] and David Komander[6#%]

[1] CRUK Therapeutic Discovery Laboratories, London Bioscience Innovation Centre, London, NW1 0NH, UK.
[2] FORMA Therapeutics, Arsenal Street, Watertown, MA 02472, U.S.A.
[3] Target Discovery Institute, Nuffield Department of Medicine, University of Oxford, Roosevelt Drive, Oxford, OX3 7FZ, UK.
[4] CRUK Therapeutic Discovery Laboratories, Jonas Webb Building, Babraham Research Campus, Cambridge, CB22 3AT, UK.
[5] Cellular and Molecular Physiology, Institute of Translational Medicine, University of Liverpool, Crown Street, Liverpool L69 3BX, UK.
[6] Medical Research Council Laboratory of Molecular Biology, Francis Crick Avenue, Cambridge, CB2 0QH, UK.

[$] Present addresses:
Goldfinch Bio, Cambridge MA, USA (S.M.B.); University of Chicago, USA (T.C.); King's College London, UK (N.J.E); Trinity College Dublin, Ireland (J.F.M.); University College London, UK (H.C.); CRUK Centre for Drug Development, London, UK (M.S.P); University of East London, UK (T.M.R.); Tarveda Therapeutics, Watertown MA, USA (M.S.); Athelas Therapeutics, Wellesley MA, USA (K.W.B.).

[%] Current steering committee of the DUB Alliance
* These authors contributed equally to this work.

Corresponding authors: Andrew P. Turnbull, Andrew.Turnbull@cancer.org.uk; Stephanos Ioannidis, sioannidis@formatherapeutics.com; Benedikt M. Kessler, benedikt.kessler@ndm.ox.ac.uk; David Komander, dk@mrc-lmb.cam.ac.uk

Word count: *Title – 64 characters; abstract - 148 words; Main text - 2341 words; Notes - 405 words; Figure legends - 667 words; 5 Figures; 43 references.*
8 Extended Data Figures, 2 Extended Data Tables, Online methods – 6514 words, 5 Methods References. 2 Supplementary Figures, 3 Supplementary Tables.

Ubiquitination controls the stability of most cellular proteins, and its deregulation contributes to human diseases including cancer. Deubiquitinases (DUBs) remove ubiquitin from proteins, and their inhibition can induce degradation of select proteins, potentially including otherwise 'undruggable' targets. For example, inhibition of ubiquitin-specific protease 7 (USP7) results in degradation of the oncogenic E3 ligase MDM2, leading to re-activation of the tumour suppressor p53 in various cancers. We here present two compounds, FT671 and FT827, that inhibit USP7 with high affinity and specificity *in vitro* and in cells. Co-crystal structures reveal that both compounds target a dynamic pocket near the catalytic centre of the auto-inhibited apo-form of USP7, which differs from other USP DUBs. Consistent with USP7 target engagement in cells, FT671 destabilises USP7 substrates including MDM2, elevates p53 and results in transcription of p53 target genes, induction of the tumour suppressor p21, and tumour growth inhibition *in vivo*.

The transcription factor p53 is an important tumour suppressor that is lost or mutated in >50% of human cancers, and multiple oncogenic mechanisms lead to its degradation by the proteasome[1,2]. Consequently, stabilisation and (re-)activation of p53 is a key aim of pharmaceutical research. One strategy focuses on targeting the oncogenic ubiquitin E3 ligase MDM2, which binds, ubiquitinates, and destabilises p53[2,3]. Inhibitors such as Nutlins prevent the MDM2-p53 interaction and p53 loss, with encouraging pre-clinical results[2].

MDM2 is protected from autoubiquitination and degradation by the deubiquitinase USP7[4,5], and genetic or chemical interference with USP7 function destabilises MDM2 and elevates p53 levels[4-6]. Small molecule inhibitors have been reported that target USP7 with a relatively narrow dynamic range (20-40 μM for P22077/P5091 and 25-50 μM for HBX41108). While they also inhibit related and unrelated enzymes[7-9], treatment with P22077/P5091 leads to MDM2 destabilisation and p53 stabilisation[8,10-14], resulting in tumour cell death *in vivo*[15-17]. P5091 is able to overcome resistance to proteasome inhibition

by bortezomib in multiple myeloma cells that overexpress USP7[12]. Consequently, these compounds reduce medulloblastoma, colorectal and lung tumour growth in mice[13,18,19], but it is unclear whether these effects are solely attributable to USP7 target modulation.

Discovery of specific USP7 inhibitors

We identified USP7 inhibitors using a ubiquitin-rhodamine assay[20], screening the inhibitory potential of a diverse collection of ~500K compounds available at FORMA Therapeutics[21]. From this, we identified several primary hits that were further validated for direct USP7 binding by biophysical techniques such as surface plasmon resonance (SPR). Optimisation of the original hits with respect to activity and physicochemical properties resulted in the prioritisation of a pyrazolo[3,4-d]pyrimidin-4-one-piperidine (PyrzPPip) series[21]. Within the series, we identified a covalent inhibitor, FT827, and a non-covalent inhibitor, FT671 (**Fig. 1a**). FT671 and FT827 bind to the USP7 catalytic domain ($USP7_{CD}$; residues 208-560, **Extended Data Fig. 1a**) with apparent K_d values of 65 (45-92) nM and 7.8 (5.9-10.2) µM, respectively (**Extended Data Fig. 1b**). FT671 inhibits USP7 with IC_{50} values of 52 (29-94) nM ($USP7_{CD}$) and 69 (39-120) nM ($USP7_{C\text{-}term}$, residues 208-1102) (**Extended Data Fig. 1c**). FT827 features a vinylsulfonamide moiety that covalently modifies the catalytic Cys223 of USP7 and inhibits the enzyme with a k_{inact}/K_I of 66 $\pm$ 25 $M^{-1}s^{-1}$ (**Fig. 1a, Extended Data Fig. 1d, Methods**). FT671 and FT827 exclusively inhibit USP7 in a panel of 38 DUBs from diverse families (**Fig. 1b, Extended Data Table 1**). We also tested FT671 against USP47 and USP10, two enzymes inhibited by P5091/P22077[7,9], but found no effect on their activity (**Extended Data Table 1**).

To test compound specificity in a cellular context, we incubated FT827 or FT671 with either crude cell extracts or with intact MCF7 breast cancer cells, followed by incubation with the ubiquitin active site suicide probe HA-UbC2Br[22] (**Fig. 1c, d, Extended Data Fig. 2a**, see **Methods**). Both compounds inhibited USP7 probe reactivity with IC_{50}s of ~0.1-2 µM, confirming 10 to 100-fold higher potency as compared to P22077 (**Extended Data Fig. 2g**). Immunoblotting for the HA-tag qualitatively indicated that no other DUB was affected (**Extended Data Fig. 2**), which was confirmed by mass-spectrometry (MS) experiments[7,23]. For this, HA-UbC2Br-modified DUBs were immunoprecipitated by anti-HA antibody, and out of 36 endogenous DUBs identified, 22 were of sufficient abundance to enable quantitative

measurements (**Fig. 1e, f, Extended Data Fig. 2a,f**). FT671 or FT827 only affected USP7, but not other DUBs including USP47 and USP10 (**Fig. 1e, f, Supplementary Tables 1, 2**). Hence, FT827 and FT671 are *bona fide* USP7-specific inhibitors.

Structures of USP7-inhibitor complexes

To understand the mechanism and specificity of USP7 inhibitors, $USP7_{CD}$ crystals were soaked with FT671 and FT827 and co-crystal structures were determined to 2.35 and 2.33 Å resolution, respectively (**Fig. 2a, Extended Data Fig. 3, Extended Data Table 2**). The USP7 catalytic domains adopt the well-characterised hand-like structure with Thumb, Fingers, and Palm subdomains[24] (**Fig. 2a**), and compounds bind in the Thumb-Palm cleft that guides the ubiquitin C-terminus into the active site (**Fig. 2a-e**). Identical interactions occur between the PyrzPPip scaffold and Asp295, Val296 (backbone), Gln297 from the Thumb subdomain, Phe409 (backbone) and Tyr465 of the Palm subdomain (**Fig. 2d, e, Extended Data Fig. 4**). The PyrzPPip scaffold of non-covalent FT671 (**Fig. 2d**) is extended towards the Fingers subdomain by a para-fluorophenyl group, and towards the catalytic centre by a 3-fluoropyrazole group that packs against the piperidine group and resides 4.7 Å from the thiol side chain of catalytic Cys223. The covalent compound FT827 (**Fig. 2e**) is not extended towards the Fingers subdomain, but is elongated towards the catalytic centre, enabling the vinylsulfonamide moiety to form a covalent bond with Cys223.

The inhibitor structures highlight the plasticity of USP7, which is known to undergo significant structural changes upon ubiquitin binding[24]. The catalytic Cys223 moves from an incompetent (apo USP7) to a catalytically competent conformation in complex with e.g. ubiquitin aldehyde (UbAl) (**Fig. 2b, c**). Further changes in the ubiquitin binding channel, in particular rotation of a Phe side chain (Phe409 in USP7, **Fig. 2b-f**), open a hydrophobic pocket that is occupied by ubiquitin Leu73 [24] (**Fig. 2c**). Similar conformations of the Phe409-equivalent residue are observed in all published USP structures (see below, **Fig. 2g**).

FT671 and FT827 bind to the inactive apo state of USP7, which is reflected by lower RMSD values of compound-bound vs. USP7-apo (0.4 Å) as compared to compound-bound vs. USP7~UbAl structures (0.8-1 Å, a ~ indicates a covalent complex) (**Fig. 2b-e, 3a**). In the USP7~FT827 structure, the compound has modified the incompetent conformation of

Cys223 despite the lack of the deprotonating activity of His464, and Phe409 is in the apo conformation (**Fig. 2e, f**). Even more striking is the Phe409 conformation in USP7-FT671, in which the compound has expelled Phe409 to a solvent exposed conformation not observed previously (**Fig. 2d, f**). This highlights surprising plasticity in USP domains whereby one of our compounds occupies a pocket not present in either the apo- or in ubiquitin-bound USP7 structures. Together, the structures explain the high affinity binding properties of FT671 and FT827, and the location in the ubiquitin binding site explains their mechanism of action as ubiquitin-competitive small molecules.

Molecular basis for compound specificity

The structures further reveal the molecular basis for compound specificity towards USP7 (**Fig. 3, Extended Data Fig. 5**). USP7 residues that mediate interactions to the inhibitors (Asp295, Val296, Gln297, Phe409, Tyr465) are highly conserved in the majority of USP enzymes[25], and sequence differences in the compound binding site alone do not explain compound specificity. Instead, the reason for the specificity lies in unique structural features of the USP7 Thumb subdomain, which harbours an allosteric regulatory interaction site known as the switching loop (**Fig. 3a**). This loop, located between helices α4 and α5 (residues 283-295), allows sufficient space for compound binding in apo USP7. Importantly, the switching loop changes upon ubiquitin binding[24], when a helical turn straightens and complements the extended ubiquitin C-terminus (**Fig. 3a, 2c**). In the ubiquitin-bound conformation, new hydrogen bonds between Tyr465 and Tyr514 of the Palm, and Asp295-Val296 of the switching loop are formed, which rigidifies the ubiquitin binding channel. These Palm-Tyr:Thumb contacts are highly conserved, and importantly, are already formed in all other apo USP structures reported to date (**Extended Data Fig. 5b**), i.e. in the absence of ubiquitin. Indeed, pre-formed Palm-Tyr:Thumb contacts and competent catalytic triad residues appear to poise other USPs for ubiquitin binding (**Extended Data Fig. 5b**).

Here, USP7 is distinct: the switching loop conformation in apo USP7 disallows a Tyr465 Thumb interaction (distance 7.9 Å), and the rotated Tyr465 side chain is free to form a hydrogen bond with the compound (**Fig. 2b, d, e, 3a, c, Extended Data Fig. 4, 5**). The unrestrained conformation of Tyr465 allows nearby Tyr514 to sit flat in the ubiquitin binding channel (**Fig. 3c, d**), and, in contrast to other USPs, this residue does not interact with the

switching loop. Both Tyr conformations create space for compound binding. In all other USP structures, equivalent Tyr residues point into the ubiquitin binding channel, which would prevent interactions with our compounds (**Fig. 3c-e, Extended Data Fig. 5b**). Together, unique positions of Tyr465 and Tyr514 in the ubiquitin binding channel, enabled by a unique conformation of the switching loop in apo USP7, allow FT671 and FT827 to specifically target USP7.

Characterisation of compound binding

Compound binding modes were tested by mutational analysis, with the aim to identify compound resistant USP7 mutants. This was challenging, since most residues involved in compound binding are also involved in ubiquitin binding and/or catalysis, and mutations had detrimental effects on USP7 function. For example, mutation of Tyr465, which forms a hydrogen bond with compound (**Fig. 2d-e, Fig. 3c-e**, see above), abrogated compound binding without affecting ubiquitin interaction as assessed by SPR (**Extended Data Fig. 6a-d**). However, while folded (**Extended Data Fig. 6e**), the $USP7_{CD}$ Y465N mutant showed a greatly reduced catalytic efficiency (k_{cat}) (**Fig. 3f, Extended Data Fig. 6f**), rendering it less useful for further analysis. Interestingly, USP7 Q297A, which removes the hydrogen bond with the compound's pyrazolo-pyrimidin-4-one group (**Fig. 3e**), retains ubiquitin binding and some catalytic activity (**Fig. 3f, Extended Data Fig. 6c, 6f**), but compound binding and inhibition is abrogated (**Fig. 3g, Extended Data Fig. 6a-b, 6d**). Finally, we examined the importance of the switching loop directly by mutating Phe291, which does not contact the compounds, but is important for the integrity of the switching loop in apo USP7 (**Fig. 3e**). Also $USP7_{CD}$ F291N showed strongly reduced compound binding and inhibition (**Fig. 3g, Extended Data Fig. 6a, 6b**), but, in contrast to the other mutants, and in agreement with previous work[26], showed improved ubiquitin affinity and ubiquitin-rhodamine activity (**Fig. 3f, Extended Data Fig. 6c, d, f**). This supports the notion that mutations in Phe291 shift the equilibrium towards an active USP7 conformation[26]. The switching loop is a point of intrinsic allosteric regulation of USP7 via its own C-terminal region and activating proteins such as $GMPS^{26-2930}$ (**Extended Data Fig. 6g**). Importantly, FT671 binds and inhibits both $USP7_{CD}$ and the more active $USP7_{C\text{-}term}$ with identical parameters *in vitro* (**Extended Data Fig. 1c**), and both compounds engage endogenous USP7 in cells (**Fig. 1c-f, Extended Data Fig. 2**). This indicates that USP7 cycles through apo-like structures that can be targeted by our compounds.

Biological activity of FT671

Cell lines derived from colorectal carcinoma (HCT116) or bone osteosarcoma (U2OS) respond to USP7 knock-down with p53 stabilisation and p21 induction, leading to growth arrest and apoptosis (**Extended Data Fig. 7a, b**). Similarly, FT671 increases p53 protein levels in these cell lines (**Fig. 4a, b**), leading to induction of p53 target genes including *BBC3*/PUMA, *CDKN1A*/p21, *RPS27L*/S27L and *MDM2* (**Fig. 4c, Extended Data Fig. 7c**). The increase in p53 correlates with increased MDM2 degradation, which is initially balanced by p53-induced MDM2 expression[31,32] but impacts on MDM2 protein levels after prolonged compound treatment (**Fig. 4a, Extended Data Fig. 7d**). Overall, these effects are similar to what has been observed with less specific compounds[12,13,18,19]. To verify that the effects on p53 arises from USP7 inhibition, we exploited compound resistant mutants (**Fig. 3e-g**). Stable HCT116 cell lines expressing a single additional copy of USP7 WT or USP7 mutants via a Flp-In TRex system, showed identical p53 induction in control and USP7 WT expressing cells upon FT671 treatment, but failed to induce p53 when USP7 Q297A or USP7 F291N were expressed (**Fig. 4d, Extended Data Fig. 7e**).

Numerous substrates of USP7 have been reported, and may be modulated by USP7 inhibition[33-35]. Indeed, FT671 led to the degradation of N-Myc and upregulation of p53 in the neuroblastoma cell line IMR-32, consistent with a previous report[33] (**Extended Data Fig. 7f**). USP7 is also part of a demethylase complex, and regulates the E3 ligase UHRF1 and the DNA methylase DNMT1[34,35]. FT671 leads to degradation of both proteins (**Extended Data Fig. 7g,h**), showing that their regulation depends on USP7 activity. As such, USP7 inhibitors appear suitable to study a variety of other biological contexts.

Physiological responses to FT671

As for other cell lines, FT671 also stabilises p53 in the MM.1S multiple myeloma cell line (**Extended Data Fig. 8a**), which correlates with increased MDM2 ubiquitination (**Extended Data Fig. 8b**) and leads to expression of p53 target genes (**Extended Data Fig. 8c, d**). FT671 blocks proliferation of MM.1S cells with an IC_{50} of 33 nM as determined by CellTiter-Glo assay (**Fig. 5a**). To test FT671 effects on the p53-MDM2 axis *in vivo*, we utilised a MM.1S xenograft mouse model in which NOD-SCID mice were implanted with MM.1S cells and randomized into different treatment groups. For pharmacodynamics studies, compound was administered once-a-day (QD) at 25 mg kg^{-1}, 75 mg kg^{-1} or 200 mg kg^{-1} via oral gavage.

Individual mice were sacrificed at different time points, and compound effects on p53 were monitored (**Fig. 5b, Extended Data Fig. 8e**). Mirroring the studies in cell lines (**Fig. 4, Extended Data Fig. 8a-d**), p53 stabilisation in tumour tissue was observed shortly after a single dose of FT671 (**Fig. 5b**). After 24 h, p53 levels have returned to those of the vehicle treated control (**Fig. 5b, Extended Data Fig. 8e**).

The *in vivo* anti-tumour growth activity of FT671 was tested in the MM.1S xenograft model after daily dosing via oral gavage at 100 mg kg^{-1} and 200 mg kg^{-1}. Treatment of mice with FT671 led to significant dose-dependent tumour growth inhibition (**Fig. 5c**). FT671 was well tolerated even at high doses, and no significant weight loss or cachexia was observed during the study (**Fig. 5d**).

Conclusion

Together, our identification of highly specific USP7 inhibitors including the nanomolar-potency, non-covalent compound FT671, shows that USPs are tractable drug targets for cancer and also other diseases[36,37]. The underlying concepts of targeting otherwise intractable, 'undruggable' proteins by modulating their half-life, is an important emerging concept in drug discovery[38,39]. It has been unclear whether the structurally highly similar USP DUBs would be amenable to the discovery of specific small molecules. We here show not only that this is possible, but also that the remarkably dynamic USP catalytic domain reveals interaction sites for small molecules that could not have been predicted from available structures. The generation of similarly selective inhibitors for other family members will unveil the full therapeutic potential of DUB inhibitors.

Acknowledgements

We thank Diamond Light Source for access to beamlines I03 and I04. We thank Susan M. Boyd for providing **Extended Data Fig. 4**, and Saosan Suhrawardy, Victoria Smith and Zhanru Yu for help with experiments. Work in the DK lab is supported by the Medical Research Council [U105192732], the European Research Council [309756], and the Lister Institute for Preventive Medicine. Work in the BMK lab was supported by a John Fell Fund 133/075, the Wellcome Trust (097813/Z/11/Z) and the Engineering and Physical Sciences Research Council (EP/N034295/1). L.S. received a stipend from North West Cancer Research.

Author contributions:

This study was directed by T.R.H., S.K., S.I., C.J.D., K.W.B., J.A.E., S.B.M., T.M.R., M.S., S.U., M.J.C., B.M.K. and D.K.. S.I. led the chemistry supported by C.J.D. and K.W.B.. Synthetic routes and approaches were devised and carried out by B.C.F., A.C.T., A.J.B. with computational chemistry support by D.R.L., J.A.C., M.W., C.L.M. and A.V.T.. USP7 biochemical assays were developed and performed by C.L.M, A.C.L.M., L.M.T., C.A and F.S.. USP10 and USP47 assays were performed by C.L.M.. A.P-F. carried out compound specificity studies and quantitative mass spectrometry using methods established by T.M.C., H.C. and J.F.M. under guidance of B.M.K. Biophysical studies were performed by; surface plasmon resonance: A.C.L.M. and L.M.T.; circular dichroism: L.M.T.; k_{inact}/K_I: A.C.L.M. using methods established by F.S.. A.P.T. and W.W.K. performed the structural studies and analysis with input from D.R.L., A.V.T., N.J.E., M.G. and D.K.. M.S.P. and L.M.T. produced protein for all experiments with input from L.M.D.S.. Biological studies were designed and performed by C.H. with the help of L.S. under guidance of S.U. and M.J.C., and carried out independently by L.S., C.G.M., E.C.T., S.M.B., J.L., M.W., M.S. under guidance of S.I. and S.K.. V.V.Z. carried out antiproliferative assay in MM.1S cells. J.L. and E.W. designed and supervised in vivo animal studies performed at Pharmaron, China. D.K., B.M.K., A.P.T. and S.I. wrote the manuscript, and all authors commented on the text.

Author information

A.P.T., W.W.K., A.C.L.M., L.M.T., N.J.E., C.A., F.S., M.S.P., T.M.R., L.M.D.S., S.B.M., T.R.H. are employees of CRUK Therapeutic Discovery Laboratories. S.I., E.C.T., S.M.B., D.R.L., J.A.C.,

A.V.T., J.L., E.W., B.C.F., V.V.Z., A.C.T., A.J.B., M.W., C.L.M., C.G.M., M.S., J.A.E., K.W.B., C.J.D. S.K. are employees of FORMA Therapeutics. This work was performed by the DUB Alliance and funded by FORMA Therapeutics.

Correspondence and requests for material should be addressed to dk@mrc-lmb.cam.ac.uk or benedikt.kessler@ndm.ox.ac.uk. Compound requests should be addressed to sioannidis@formatherapeutics.com.

References

1. Kruiswijk, F., Labuschagne, C. F. & Vousden, K. H. p53 in survival, death and metabolic health: a lifeguard with a licence to kill. *Nat Rev Mol Cell Biol* **16,** 393–405 (2015).
2. Wade, M., Li, Y.-C. & Wahl, G. M. MDM2, MDMX and p53 in oncogenesis and cancer therapy. *Nat Rev Cancer* **13,** 83–96 (2013).
3. Khoo, K. H., Hoe, K. K., Verma, C. S. & Lane, D. P. Drugging the p53 pathway: understanding the route to clinical efficacy. *Nat Rev Drug Discov* **13,** 217–236 (2014).
4. Cummins, J. M. *et al.* Tumour suppression: disruption of HAUSP gene stabilizes p53. *Nature* **428,** 1 p following 486 (2004).
5. Li, M., Brooks, C. L., Kon, N. & Gu, W. A dynamic role of HAUSP in the p53-Mdm2 pathway. *Mol Cell* **13,** 879–886 (2004).
6. Li, M. *et al.* Deubiquitination of p53 by HAUSP is an important pathway for p53 stabilization. *Nature* **416,** 648–653 (2002).
7. Altun, M. *et al.* Activity-based chemical proteomics accelerates inhibitor development for deubiquitylating enzymes. *Chem Biol* **18,** 1401–1412 (2011).
8. Weinstock, J. *et al.* Selective Dual Inhibitors of the Cancer-Related Deubiquitylating Proteases USP7 and USP47. *ACS Med Chem Lett* **3,** 789–792 (2012).
9. Ritorto, M. S. *et al.* Screening of DUB activity and specificity by MALDI-TOF mass spectrometry. *Nature Communications* **5,** 4763 (2014).
10. Colland, F. *et al.* Small-molecule inhibitor of USP7/HAUSP ubiquitin protease stabilizes and activates p53 in cells. *Mol. Cancer Ther.* **8,** 2286–2295 (2009).
11. Reverdy, C. *et al.* Discovery of specific inhibitors of human USP7/HAUSP deubiquitinating enzyme. *Chem Biol* **19,** 467–477 (2012).
12. Chauhan, D. *et al.* A small molecule inhibitor of ubiquitin-specific protease-7 induces apoptosis in multiple myeloma cells and overcomes bortezomib resistance. *Cancer Cell* **22,** 345–358 (2012).
13. Wang, L. *et al.* Ubiquitin-specific Protease-7 Inhibition Impairs Tip60-dependent Foxp3+ T-regulatory Cell Function and Promotes Antitumor Immunity. *EBioMedicine* **13,** 99–112 (2016).
14. Yamaguchi, M. *et al.* Spongiacidin C, a pyrrole alkaloid from the marine sponge Stylissa massa, functions as a USP7 inhibitor. *Bioorg. Med. Chem. Lett.* **23,** 3884–3886 (2013).
15. Dar, A., Shibata, E. & Dutta, A. Deubiquitination of Tip60 by USP7 determines the activity of the p53-dependent apoptotic pathway. *Mol Cell Biol* **33,** 3309–3320 (2013).
16. Fan, Y.-H. *et al.* USP7 inhibitor P22077 inhibits neuroblastoma growth via inducing p53-mediated apoptosis. *Cell Death Dis* **4,** e867 (2013).

17. Lee, G. *et al.* Small-molecule inhibitors of USP7 induce apoptosis through oxidative and endoplasmic reticulum stress in cancer cells. *Biochem Biophys Res Commun* **470,** 181–186 (2016).
18. An, T. *et al.* USP7 inhibitor P5091 inhibits Wnt signaling and colorectal tumor growth. *Biochem Pharmacol* **131,** 29–39 (2017).
19. Zhan, M. *et al.* Usp7 promotes medulloblastoma cell survival and metastasis by activating Shh pathway. *Biochem Biophys Res Commun* **484,** 429–434 (2017).
20. Hassiepen, U. *et al.* A sensitive fluorescence intensity assay for deubiquitinating proteases using ubiquitin-rhodamine110-glycine as substrate. *Anal. Biochem.* **371,** 201–207 (2007).
21. Ioannidis, S. *et al.* Pyrrolo and pyrazolopyrimidines as ubiquitin-specific protease 7 inhibitors. US Patent WO2016109515 (2015).
22. Borodovsky, A. *et al.* Chemistry-based functional proteomics reveals novel members of the deubiquitinating enzyme family. *Chem Biol* **9,** 1149–1159 (2002).
23. McGouran, J. F., Gaertner, S. R., Altun, M., Kramer, H. B. & Kessler, B. M. Deubiquitinating enzyme specificity for ubiquitin chain topology profiled by di-ubiquitin activity probes. *Chem Biol* **20,** 1447–1455 (2013).
24. Hu, M. *et al.* Crystal structure of a UBP-family deubiquitinating enzyme in isolation and in complex with ubiquitin aldehyde. *Cell* **111,** 1041–1054 (2002).
25. Ye, Y., Scheel, H., Hofmann, K. & Komander, D. Dissection of USP catalytic domains reveals five common insertion points. *Mol Biosyst* **5,** 1797–1808 (2009).
26. Faesen, A. C. *et al.* Mechanism of USP7/HAUSP activation by its C-terminal ubiquitin-like domain and allosteric regulation by GMP-synthetase. *Mol Cell* **44,** 147–159 (2011).
27. Rouge, L. *et al.* Molecular Understanding of USP7 Substrate Recognition and C-Terminal Activation. *Structure* **24,** 1335–1345 (2016).
28. Kim, R. Q., van Dijk, W. J. & Sixma, T. K. Structure of USP7 catalytic domain and three Ubl-domains reveals a connector α-helix with regulatory role. *J Struct Biol* **195,** 11–18 (2016).
29. van der Knaap, J. A. *et al.* GMP synthetase stimulates histone H2B deubiquitylation by the epigenetic silencer USP7. *Mol Cell* **17,** 695–707 (2005).
30. Kim, R. Q. & Sixma, T. K. Regulation of USP7: A High Incidence of E3 Complexes. *J Mol Biol* (2017). doi:10.1016/j.jmb.2017.05.028
31. Barak, Y., Juven, T., Haffner, R. & Oren, M. mdm2 expression is induced by wild type p53 activity. *EMBO J* (1993).
32. Wu, X., Bayle, J. H., Olson, D. & Levine, A. J. The p53-mdm-2 autoregulatory feedback loop. *Genes Dev* **7,** 1126–1132 (1993).
33. Tavana, O. *et al.* HAUSP deubiquitinates and stabilizes N-Myc in neuroblastoma. *Nat Med* **22,** 1180–1186 (2016).
34. Felle, M. *et al.* The USP7/Dnmt1 complex stimulates the DNA methylation activity of Dnmt1 and regulates the stability of UHRF1. *Nucleic Acids Res* **39,** 8355–8365 (2011).
35. Du, Z. *et al.* DNMT1 Stability Is Regulated by Proteins Coordinating Deubiquitination and Acetylation-Driven Ubiquitination. *Sci. Signal.* **3,** ra80–ra80 (2010).
36. Clague, M. J. *et al.* Deubiquitylases from genes to organism. *Physiol. Rev.* **93,** 1289–1315 (2013).
37. Cohen, P. & Tcherpakov, M. Will the Ubiquitin System Furnish as Many Drug Targets as Protein Kinases? *Cell* **143,** 686–693 (2010).

38. Salami, J. & Crews, C. M. Waste disposal—An attractive strategy for cancer therapy. *Science* **355,** 1163–1167 (2017).
39. Huang, X. & Dixit, V. M. Drugging the undruggables: exploring the ubiquitin system for drug development. *Cell Res* **26,** 484–498 (2016).
40. Clerici, M., Luna-Vargas, M. P. A., Faesen, A. C. & Sixma, T. K. The DUSP-Ubl domain of USP4 enhances its catalytic efficiency by promoting ubiquitin exchange. *Nature Communications* **5,** 5399 (2014).
41. Avvakumov, G. V. *et al.* Amino-terminal dimerization, NRDP1-rhodanese interaction, and inhibited catalytic domain conformation of the ubiquitin-specific protease 8 (USP8). *J Biol Chem* **281,** 38061–38070 (2006).
42. Li, H. *et al.* Allosteric Activation of Ubiquitin-Specific Proteases by β-Propeller Proteins UAF1 and WDR20. *Mol Cell* **63,** 249–260 (2016).
43. Hu, M. *et al.* Structure and mechanisms of the proteasome-associated deubiquitinating enzyme USP14. *EMBO J* **24,** 3747–3756 (2005).

Figure 1. Properties and specificity of small molecule USP7 inhibitors.

a, Structures of FT671 (top) and FT827 (bottom) containing a PyrzPPip scaffold (red) and key inhibitor parameters (see **Extended Data Fig. 1**). **b,** Commercial DUB specificity screen (one replicate) with 50 µM FT671 and FT827. **c-d,** Cell lysates (**c**) or intact MCF7 cells (**d**) were incubated with FT671 or FT827, then with HA-UbC2Br probes. Modification of USP7 with ubiquitin probe (USP7~Ub) was lost with increasing concentrations of inhibitors. One of two independent biological experiments is shown (see **Extended Data Fig. 2**). **e-f,** HA-based immunoprecipitation of labelled DUBs from experiments in **c** were subjected to mass spectrometry (MS)-based quantification in three technical replicates[7]. Differences in DUB-probe binding were quantified for 22 out of 36 identified DUBs (see **Supplementary Tables 1, 2**). FT827 or FT671 only affect USP7 (see **Methods** for statistics). Uncropped images for gels are shown in **Supplementary Figure 1.**

Figure 2. USP7-inhibitor complex structures.

a, Overall structure of USP7 apo (1NB8[24]), USP7-FT671, USP7~FT827 (compounds shown under yellow surface), and USP7~UbAl (1NBF[24]). See **Extended Data Fig. 3, 4** and **Extended Data Table 2**. **b-e**, Close-up view of the compound binding site highlighting key residues. **b,** apo USP7; **c**, USP7~UbAl; **d**, USP7-FT671; **e,** USP7~FT827. See also **Extended Data Fig. 4**. **f**, Close-up view of the different conformations of Phe409 from **b-e**. **g**, Superposition of reported USP apo (*top*) and ubiquitin-bound (*bottom*) structures showing conserved Phe and Tyr residues.

Figure 3. Molecular basis of selective USP7 inhibition.

a, Superposition of USP7 apo, USP7-FT671, USP7~FT827 and USP7~UbAl structures, showing that compounds target the apo conformation. **b**, Superposition of USP apo structures onto USP7-FT671. See also **Extended Data Fig. 5a**. **c**, Superposition of USP7 apo onto USP7-FT671 (*left*) and apo USP4 (2Y6E [40], *right*), explaining the positions of key Tyr residues. See also **Extended Data Fig. 5b**. **d**, View highlighting steric clashes between Tyr residues and compound in USP4. **e**, Compound resistant mutant positions (orange). **f**, K_M and k_{cat} determination for USP7 wild-type and mutants (n=3 biological, n=5 technical replicates). See **Extended Data Fig. 6f**. Mutants are folded (**Extended Data Fig. 6e**). **g**, Compound inhibition for wild-type USP7 and indicated mutants. (n=3 biological, n=3 technical replicates).

Figure 4. Effects of USP7 inhibitor FT671 in cell lines.

a, HCT116 cells were treated with FT671 for 20 h, and cell lysates assessed by Western blotting. One out of three biological replicates is shown. **b**, U2OS cells were treated with 0.1-10 μM FT671 for 20 h and analysed as above. One out of two biological replicates is shown. **c**, HCT116 cells were treated with 10 μM FT671 for 24 h and RNA extracted for real-time PCR measurements with primer sets against indicated transcripts (see **Methods**). Experiments were performed in biological triplicate (duplicate for *RPS27L*). **d,** Expression of USP7 variants in HCT116 Flip-In TRex cells was induced for 7 h with 0.1 μg/mL doxycycline followed by treatment with 1 μM FT671 or vehicle for the last 4 h. One out of two biological replicates is shown. Uncropped images for gels are shown in **Supplementary Figure 1.**

Figure 5. Physiological response to USP7 specific inhibitor FT671

a, MM.1S cells were treated with increasing amounts of FT671 and viability of cells was assessed after 120 h using the CellTiter-Glo assay. The graph displays three biological replicates, each point representing the mean of three technical replicates. **b**, Analysis of p53 levels in MM.1S tumour xenografts after a single 200 mg kg^{-1} dose of FT671 in comparison to the vehicle treated xenografts (unpaired, two-tailed *Student's* t-test). Data represents Mean +/- Standard Deviation (SD) from n=5. See **Extended Data Fig. 8e** for the corresponding Western blots. **c**, MM.1S tumour growth was significantly reduced in a dose dependent manner by daily treatment with FT671 (2-way ANOVA). The data represents Mean +/- SD from n=9 replicates. See **Methods** for statistical analysis. **d**, Analysis of body weight during daily treatment of MM.1S xenograft bearing mice with 100 mg kg^{-1} or 200 mg kg^{-1} FT671. Data represent Mean +/- SD (SEM) from n=9 replicates.

Online Methods

Protein expression and purification for $USP7_{CD}$ proteins

His-tagged $USP7_{CD}$ (residues 208-560) and the corresponding F291N and Q297A point mutation constructs were cloned into the pETNHT-1 vector and expressed in *E.coli* Rosetta2 cells. Cells were grown in TB at 37 °C to an OD_{600} of 0.6, induced with 0.5 mM IPTG and incubated overnight at 15 °C.

The cell pellet was re-suspended in lysis buffer A (50 mM HEPES pH7.5, 300 mM NaCl, 1 mM DTT, 15 mM Imidazole, 5 mM benzamidine, 1 mM AEBSF, 500 U benzonase) and lysed using a Constant Systems Ltd cell disruptor. Insoluble material was removed by centrifugation and the supernatant was loaded onto a HiTrap TALON crude column (GE Healthcare) equilibrated with Ni Buffer A (50 mM HEPES pH 7.5, 300 mM NaCl, 1 mM DTT, 15 mM imidazole) and washed with Buffer A + 45 mM imidazole until A_{280} reached baseline. The protein was eluted with Ni Buffer B (50mM HEPES pH 7.5, 300 mM NaCl, 1 mM DTT, 300 mM imidazole) and further purified using a HiLoad 26/60 Superdex 75 column (GE Healthcare) equilibrated with SEC Buffer (50 mM HEPES pH 7.5, 150 mM NaCl, 1 mM DTT). The protein was concentrated to ~20 mg ml^{-1}, flash-frozen in liquid N_2 and stored at -80 °C.

Protein expression and purification for $USP7_{C\text{-}term}$

Hi Five™ Sf9 insect cells expressing $USP7_{C\text{-}term}$ (residues 208-1102) were re-suspended in lysis buffer B (50 mM Tris pH 8.0, 200 mM NaCl, 5% (v/v) glycerol, 5 mM β-mercaptoethanol, 1 mM PMSF) and lysed using a Constant Systems Ltd cell disruptor. Insoluble material was removed by centrifugation and the supernatant was loaded onto a Ni-NTA column (GE Healthcare) equilibrated with Ni Buffer A (50 mM Tris pH 8.0, 200 mM NaCl, 5% (v/v) glycerol, 5 mM β-mercaptoethanol) and washed with Ni Buffer A + 60 mM imidazole until A_{280} reached baseline. The protein was eluted with Ni Buffer B (50 mM Tris pH 8.0, 200 mM NaCl, 5% glycerol, 5 mM β-mercaptoethanol, 250 mM imidazole). The protein was further purified using a HiLoad 16/600 Superdex 200 column (GE Healthcare) equilibrated with 50 mM Tris pH 8.0, 200 mM NaCl, 5% (v/v) glycerol, 5 mM DTT. The protein was concentrated to ~10 mg ml^{-1}, flash-frozen in liquid N_2 and stored at -80 °C.

Chemical synthesis of USP7 compounds

FT671 and FT827 were prepared in agreement with the procedures described in detail in [21]. The chemical synthesis is described below, and the characterisation data can be found in **Supplementary Figure 2a-k**.

General

^{1}H, ^{13}C and ^{19}F nuclear magnetic resonance (NMR) spectra were obtained on either Bruker or Varian spectrometers at 300 or 400 MHz, respectively. Spectra are given in ppm (δ) using the residual peak of the solvent as internal standard (DMSO-d_6: 2.50 ppm (^{1}H) / 39.5 ppm (^{13}C); CD_3OD: 3.31 ppm (1H) or tetramethylsilane (TMS) as internal standards. and coupling constants, J, are reported in Hertz. Mass spectra were collected using a Waters ZQ Single Quad Mass Spectrometer (ion trap electrospray ionization (ESI)). Purity and low resolution mass spectral data were measured using Waters Acquity i-class ultra-performance liquid chromatography (UPLC) system with Acquity Photo Diode Array Detector, Acquity Evaporative Light Scattering Detector (ELSD) and Waters ZQ Mass Spectrometer. Data was acquired using Waters MassLynx 4.1 software and purity characterized by UV wavelength 220 nm, evaporative light scattering detection (ELSD) and electrospray positive ion (ESI). (Column: Acquity UPLC BEH C18 1.7µm 2.1 X 50 mm; Flow rate 0.6mL/min; Solvent A (95/5/0.1%: 10mM Ammonium Formate/Acetonitrile/Formic Acid), Solvent B (95/5/0.09%: Acetonitrile/Water/Formic Acid); gradient: 5-100% B from 0 to 2mins, hold 100%B to 2.2mins and 5%B at 2.21mins. The absolute configuration of FT671 was assigned by X-Ray crystallography

1. Preparation of FT827

2'-aminobiphenyl-4-carboxylic acid

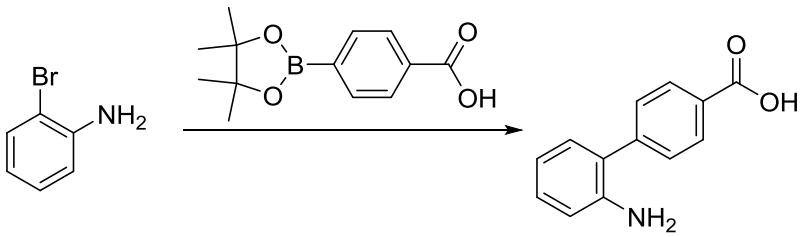

A 250-mL round-bottom flask fitted with a nitrogen balloon, magnetic stir bar, condenser and thermometer was charged with 2-bromoaniline (2 g, 11.63 mmol), dioxane (40 mL), water (4 mL), K_3PO_4 (7.6 g, 35.80 mmol), 4-(tetramethyl-1,3,2-dioxaborolan-2-yl)benzoic acid (3.2 g, 12.84 mmol) and 1,1'-bis(diphenylphosphino)ferrocene palladium(II) chloride complex with dichloromethane (0.76 g, 0.94 mmol). The resulting solution was stirred for 10 h at 100 °C under nitrogen. The reaction mixture was cooled to 25 °C. The pH of the mixture was adjusted to 5 with hydrochloric acid (6 N). The product was extracted with dichloromethane (2 x 30 mL). The organic layers were combined, dried over anhydrous sodium sulfate, filtered and concentrated under vacuum to afford 2'-aminobiphenyl-4-carboxylic acid (0.8 g, 32%). LCMS: (ES) *m/z* 214 [M+H].

5-((4-hydroxypiperidin-4-yl)methyl)-1-methyl-1H-pyrazolo[3,4-d]pyrimidin-4(5H)-one), trifluoroacetic acid salt

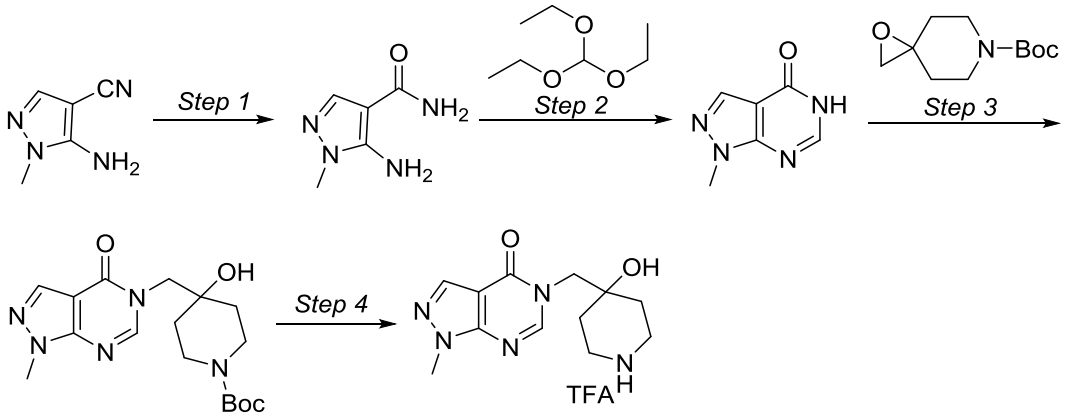

Step 1. **5-Amino-1-methyl-1*H*-pyrazole-4-carboxamide**

A 500-mL 3-necked round-bottom flask fitted with a magnetic stir bar and thermometer was charged with sulfuric acid (120 mL), followed 5-amino-1-methyl-1*H*-pyrazole-4-carbonitrile (52 g, 426 mmol) in portions at 0 °C. Upon completion of the addition, the reaction mixture was warmed to room temperature and stirred for 1 h. The reaction quenched with sodium hydroxide (50% wt solution in water) and the pH of the mixture was adjusted to 8. The solids were collected by filtration, washed with water (3 x 50 mL) and dried in an oven to provide 5-amino-1-methyl-*1H*-pyrazole-4-carboxamide (50 g, 84%). LCMS: (ESI) m/z 141 [M+H].

Step 2. **1-Methyl-1*H*-pyrazolo[3,4-d]pyrimidin-4(5H)-one**

A 500-mL 3-necked round-bottom flask fitted with a magnetic stir bar, condenser and thermometer was charged with 5-amino-1-methyl-1*H*-pyrazole-4-carboxamide (Step 1, 50 g, 357 mmol), (diethoxymethoxy)ethane (120 mL) and acetic anhydride (120 mL). The solution was stirred for 1 h at 130 °C in an oil bath. The reaction mixture was allowed to cool to 0 °C. The solids were collected by filtration, washed with *n*-hexane (3 x 50 mL) and dried in an oven to provide to 1-methyl-1*H*-pyrazolo[3,4-d]pyrimidin-4(5H)-one (51 g, 95%). LCMS: (ESI) m/z 151 [M+H].

Step 3. ***Tert*-butyl4-hydroxy-4-((1-methyl-4-oxo-1H-pyrazolo[3,4-d]pyrimidin-5 (4*H*)-yl)methyl)piperidine-1-carboxylate**

A 500-mL 3-necked round-bottom flask fitted with a magnetic stir bar, condenser and thermometer was charged with 1-methyl-1*H*-pyrazolo[3,4-d]pyrimidin-4(5H)-one (Step 2, 20 g, 133 mmol), *N,N*-dimethylformamide (150 mL), *tert*-butyl 1-oxa-6-azaspiro[2.5]octane-6-carboxylate (31 g, 146 mmol), Cs_2CO_3 (130 g, 399 mmol). The reaction mixture was stirred for 2 h at 80 °C in an oil bath. After cooling to room temperature, the reaction was quenched with water (300 mL). The product was extracted with ethyl acetate (4 x 200 mL). The combined organic layers were washed with brine (300 mL), dried over anhydrous sodium sulfate, filtered and concentrated under vacuum. The residue was purified by column chromatography eluting with dichloromethane/methanol (10:1, v/v) to yield *tert*-butyl 4-hydroxy-4-((1-methyl-4-oxo-1*H*-pyrazolo[3,4-d]pyrimidin-5(4*H*)-yl)methyl)piperidine-1-carboxylate (30 g, 62%). ^{1}H-NMR (300MHz, $CDCl_3$): δ1.45 (s, 9H), 1.47-1.67 (m, 4H), 3.12-3.19 (m, 2H), 3.96-3.81 (m, 2H), 4.00 (s, 3H), 4.04-4.18 (m, 2H), 8.02 (s, 1H), 8.07 (s, 1H) ppm. ^{13}C-NMR (101 MHz, CHLOROFORM-*d*): δ ppm 28.4, 34.3, 35.1, 55.4, 70.3, 79.7, 105.4, 135.1, 149.7, 151.5, 154.6, 158.7. LCMS: (ESI) m/z 364 [M+H].

Step 4. **5-((4-hydroxypiperidin-4-yl)methyl)-1-methyl-1*H*-pyrazolo [3,4-d]pyrimidin-4(5*H*)-one, trifluoroacetic acid salt**

A 250-mL round-bottom flask fitted with a magnetic stir bar was charged with tert-butyl 4-hydroxy-4-((1-methyl-4-oxo-1H-pyrazolo[3,4-d]pyrimidin-5(4*H*)-yl) methyl)piperidine-1-carboxylate (Step 3, 20 g, 55 mmol), trifluoroacetic acid salt (20 mL) and dichloromethane (150 mL). The solution was stirred for 4 h at room temperature and concentrated under vacuum to give 5-((4-hydroxypiperidin-4-yl)methyl)-1-methyl-1*H*-pyrazolo[3,4-d]pyrimidin-4(5*H*)-one, trifluoroacetic acid salt (21 g). LCMS: (ESI) m/z 264 [M+H].

***N*-(4'-(4-hydroxy-4-((1-methyl-4-oxo-1*H*-pyrazolo[3,4-d] pyrimidin-5(4*H*)-yl)methyl)piperidine-1-carbonyl)biphenyl-2-yl)ethenesulfonamide**

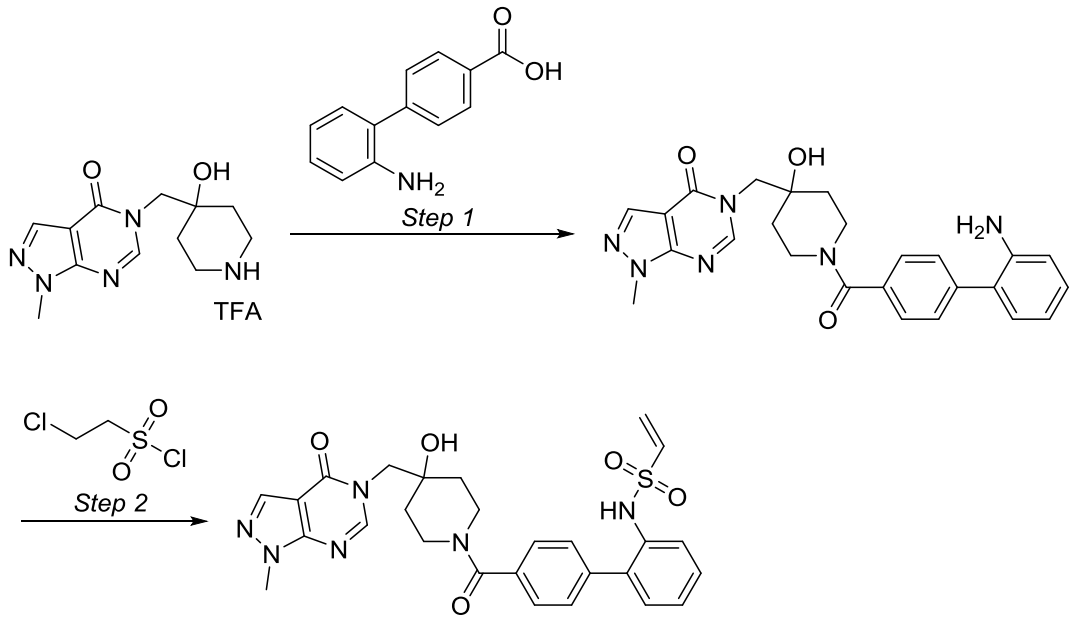

Step 1. **5-((1-(2'-Aminobiphenylcarbonyl)-4-hydroxypiperidin-4-yl)methyl)-1- methyl-1H-pyrazolo[3,4-d]pyrimidin-4(5*H*)-one**

A 100-mL round-bottom flask fitted with a magnetic stir bar was charged with 2'-aminobiphenyl-4-carboxylic acid (400 mg, 1.88 mmol), 5-((4-hydroxypiperidin-4-yl)methyl)-1-methyl-1*H*-pyrazolo[3,4-d]pyrimidin-4(5H)-one, trifluoroacetic acid salt (800 mg, 2.12 mmol) 1-[Bis(dimethylamino)methylene]-1H-1,2,3-triazolo[4,5-b]pyridinium 3-oxid hexafluorophosphate) (857 mg, 2.25 mmol), *N*,*N*-diethylisopropylamine (970 mg, 7.51 mmol) and dichloromethane (30 mL). The resulting solution was stirred for 2 h at 25 °C and then diluted with water (30 mL). The product was extracted with dichloromethane (3 x 30 mL). The combined organic layers were dried over anhydrous sodium sulfate, filtered and concentrated under vacuum. The residue was purified by preparatory thin layer chromatography eluting with ethyl acetate to afford 5-((1-(2'-aminobiphenylcarbonyl)-4-hydroxypiperidin-4-yl)methyl)-1-methyl-1*H*-pyrazolo[3,4-d]pyrimidin-4(5*H*)-one (220 mg, 26%). LCMS: (ESI) m/z 459[M+H].

Step 2. ***N*-(4'-(4-hydroxy-4-((1-methyl-4-oxo-1*H*-pyrazolo[3,4-d]pyrimidin-5(4*H*) -yl)methyl)piperidine-1-carbonyl)biphenyl-2-yl)ethenesulfonamide (FT827)**

A 100-mL 3-necked round-bottom flask fitted with a nitrogen balloon, magnetic stir bar and thermometer was charged with 5-((1-(2'-aminobiphenylcarbonyl)-4-hydroxypiperidin-4-

yl)methyl)-1-methyl-*1H*-pyrazolo[3,4-d]pyrimidin-4(5H)-one (Step 1, 40 mg, 0.09 mmol), dichloromethane (5 mL) and triethylamine (30.7 mg, 0.30 mmol). A solution of 2-chloroethane-1-sulfonyl chloride (17 mg, 0.10 mmol) in dichloromethane (1 mL) was added in portions at 0 °C. The resulting solution was stirred for 0.5 h at 0 °C and then concentrated under vacuum. The residue was purified by preparatory HPLC* to give *N*-(4'-(4-hydroxy-4-((1-methyl-4-oxo-1*H*-pyrazolo[3,4-d]pyrimidin-5(4*H*)-yl)methyl)piperidine-1-carbonyl)biphenyl-2-yl)ethenesulfonamide as a white solid (11 mg, 21%). *Column: X bridge prep shield RP18 OBD Column 19 x 150 nm, 5 µM Mobile phase A: water (0.05% NH_4HCO_3)/Mobile phase B: acetonitrile. Flow rate: 20 mL/min. Gradient: 16% B to 42% B over 7 min. Detector: 220 and 254 nm (**Supplementary Figure 2a**).

High-resolution mass spectrometry (HRMS): ($C_{24}H_{23}F_4N_7O_3$ – expected $[M+H]^+$ 549.19201, observed $[M+H]^+$ 549.19150 (0.93 ppm) (**Supplementary Figure 2b**). Agilent QTOF 6560 LC-MS ESI+ mode. Column: Waters Acquity UPLC BEH C18, 1.7 um, 2.1 x 50 mm. Mobile phase A: 95% Water/5% Acetonitrile with 0.1% Formic Acid in 10 mM Ammonium Formate/Mobile phase B: 95% Acetonitrile/5% Water with 0.09% Formic Acid. Flow rate: 20 mL/min. Column temperature: 35 °C. Gradient: 5-100% B in 2.0 min, hold 100% to 2.2 min. LC Flow Rate: 0.6 mL/min. Detector: 220 nm.

^{1}H-NMR (400MHz, CD_3OD) δ 1.46-1.64 (m, 1H), 1.68-1.87 (m, 3H), 3.46-3.49 (m, 2H), 3.68-3.72 (m, 1H), 3.99 (s, 3H), 4.12-4.21 (m, 2H), 4.38-4.41 (m, 1H), 5.88 (d, J = 10.0Hz, 1H), 6.06 (d, J = 16.8Hz, 1H), 6.50-6.54 (m, 1H), 7.31-7.40 (m, 3H), 7.46-7.56 (m, 5H), 8.06 (s, 1H), 8.28 (s, 1H) ppm (**Supplementary Figure 2c**).

^{13}C-NMR (101 MHz, CHLOROFORM-*d*): δ ppm 34.3, 55.9, 70.4, 105.4, 119.8, 124.9, 128.0, 128.5, 129.2, 129.4, 130.7, 132.1, 133.4, 135.1, 135.4, 135.8, 139.0, 149.4, 151.5, 158.9, 169.6 (**Supplementary Figure 2d,e**).

2. Preparation of FT671

4,4-difluoro-3-(1H-pyrazol-1-yl)butanoic acid

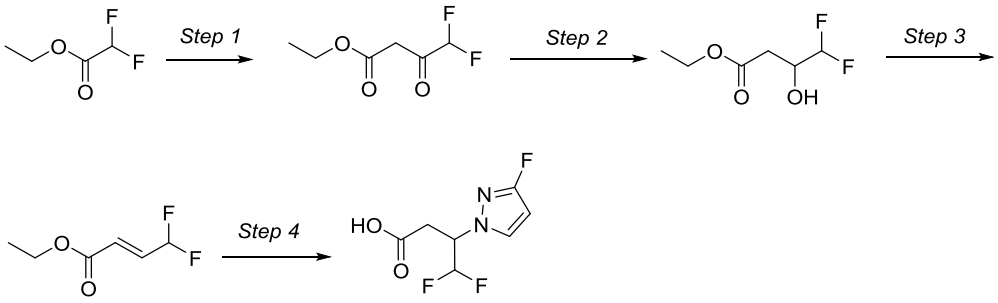

Step 1. **Ethyl 4,4-difluoro-3-oxobutanoate**

A 500-mL round-bottom flask was charged with sodium ethoxide (28.3 g, 416 mmol) and ethanol (80 mL) followed by the addition of a solution of ethyl 2,2-difluoroacetate (43 g, 347 mmol) in ethyl acetate (170 mL) added slowly with stirring at room temperature. The resulting solution was stirred for 2 h at 60 °C. Upon cooling to room temperature, the reaction was quenched by the addition of hydrochloric acid (aqueous 6N, 150 mL) and the pH of the solution was adjusted to 4-5. The resulting solution was extracted with ethyl acetate (3 x 200 mL) and the organic layers were combined and dried over anhydrous sodium sulfate and concentrated under vacuum to afford ethyl 4,4-difluoro-3-oxobutanoate which was used in Step 2 without further purification (29 g). GCMS *m/z* 166.

Step 2. **Ethyl 4,4-difluoro-3-hydroxybutanoate**

A 500-mL round-bottom flask was charged with crude ethyl 4,4-difluoro-3-oxobutanoate (Step 1, 8 g, 96 mmol), toluene (250 mL) and sodium borohydride (2.38 g, 64.63 mmol). The resulting solution was stirred for 2 h at 65 °C. The reaction was then quenched by the addition of water (100 mL). The resulting solution was extracted with ethyl acetate (3 x 50 mL) and the organic layers were combined, washed with brine, dried over anhydrous sodium sulfate and concentrated under vacuum. The residue was purified by column chromatography eluting with ethyl acetate/petroleum ether (1:5 to 1:2 v/v) to afford ethyl 4,4-difluoro-3-hydroxybutanoate (6.8 g, 35% over 2 steps). GCMS *m/z* 168.

Step 3. ***(E)*-ethyl 4,4-difluorobut-2-enoate**

A 25-mL round-bottom flask was charged with ethyl 4,4-difluoro-3-hydroxybutanoate (Step 2, 5g, 48.16 mmol) and phosphorus pentoxide (3.4 g, 23.62 mmol). The resulting solution was stirred for 2 h at 70 ^{o}C in an oil bath. The mixture was purified by distillation under

reduced pressure (1 mm Hg) and the fraction was collected at 100 °C to give (E)-ethyl 4,4-difluorobut-2-enoate as a colorless oil (1.8 g, 25%). GCMS *m/z* 150.

Step 4. **4,4-difluoro-3-(3-fluoro-1*H*-pyrazol-1-yl)butanoic acid**

A 100-mL round-bottom flask was charged with 3-fluoro-1*H*-pyrazole (102 mg, 1.50 mmol) and tetrahydrofuran (20 mL) followed by the addition of sodium hydride (52 mg, 2.17 mmol) at 0 °C. The resulting solution was stirred 30 min at 0 °C before adding (*E*)-ethyl 4,4-difluorobut-2-enoate (Step 3, 150 mg, 1.00 mmol). The resulting solution was stirred 16 h at room temperature. The reaction was quenched by the addition of 10 mL of water and extracted with ethyl acetate (30 mL). The pH of the aqueous layer was adjusted to 4-5 with aqueous hydrochloric acid (aqueous, 6 N) and extracted with dichloromethane (2 x 30 mL). The organic layers were combined, dried over anhydrous sodium sulfate and concentrated under vacuum to give 4,4-difluoro-3-(3-fluoro-1*H*-pyrazol-1-yl)butanoic acid (90 mg) as a yellow oil which was used without further purification. LCMS: (ESI) *m/z* 191 [M+H].

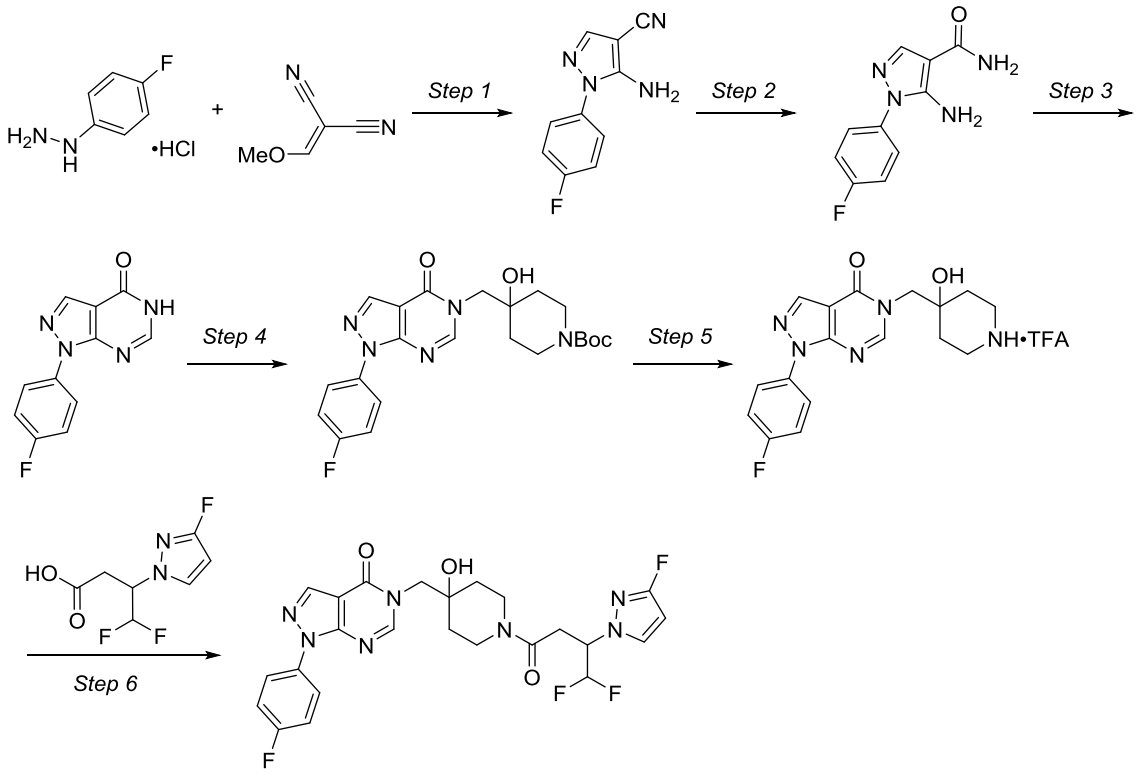

Step 1. **5-Amino-1-(4-fluorophenyl)-1*H*-pyrazole-4-carbonitrile**

2-(Methoxymethylene)malononitrile (1.00 g, 9.25 mmol), (4-fluorophenyl) hydrazine hydrochloride (1.40 g, 8.61 mmol), triethylamine (1.66 g, 16.4 mmol) and ethanol (50 mL) were added to a 100-mL round-bottom flask fitted with a magnetic stir bar and condenser.

The resulting solution was heated at reflux for 16 h. The resulting mixture was concentrated under vacuum. The residue was purified by column chromatography eluting with dichloromethane/methanol (10:1 v/v) to give 5-amino-1-(4-fluorophenyl)-1*H*-pyrazole-4-carbonitrile (1.00 g, 57 %). LCMS: (ESI) *m/z* 203 [M+H].

Step 2. **5-Amino-1-(4-fluorophenyl)-1*H*-pyrazole-4-carboxamide**

5-Amino-1-(4-fluorophenyl)-1*H*-pyrazole-4-carboxamide (Step 1, 900 mg, 4.45 mmol) was added dropwise to sulfuric acid (10 mL) at 0 ºC. The resulting solution was stirred for 2 h at 25 ºC. The pH of the solution was adjusted to 8 by the addition of 10% aqueous sodium carbonate. The resulting mixture was extracted with dichloromethane (4 x 50 mL) and the organic layers were combined, dried over anhydrous sodium sulfate, filtered and concentrated under vacuum to provide 5-amino-1-(4-fluorophenyl)-1*H*-pyrazole-4-carboxamide which was used in Step 3 without further purification. LCMS: (ESI) *m/z* 221 [M+H].

Step 3. **1-(4-Fluorophenyl)-1,5-dihydro-4*H*-pyrazolo[3,4-*d*]pyrimidin-4-one**

5-Amino-1-(4-fluorophenyl)-1*H*-pyrazole-4-carboxamide (Step 2, 1.00 g, 4.5 mmol), triethyl orthoformate (20 mL) and acetic anhydride (20 mL) were added to a 100-mL round-bottom flask fitted with a magnetic stir bar and condenser. The resulting solution was heated at reflux for 1 h and then concentrated under vacuum. The solids were collected and washed with hexane (3 x 20 mL) to afford 1-(4-fluorophenyl)-1,5-dihydro-4*H*-pyrazolo[3,4-*d*]pyrimidin-4-one which was used in Step 4 without further purification. LCMS: (ESI) *m/z* 231 [M+H].

Step 4. ***tert*-Butyl 4-((1-(4-fluorophenyl)-4-oxo-1,4-dihydro-5*H*-pyrazolo[3,4-*d*]pyrimidin-5-yl)methyl)-4-hydroxypiperidine-1-carboxylate**

1-(4-Fluorophenyl)-1,5-dihydro-4*H*-pyrazolo[3,4-*d*]pyrimidin-4-one (Step 3, 1.00 g, 4.3 mmol), *tert*-butyl 1-oxa-6-azaspiro[2.5]octane-6-carboxylate (926 mg, 4.34 mmol), cesium carbonate (4.30 g, 13.2 mmol) and DMF (50 mL) were added to a 100-mL round-bottom flask fitted with a magnetic stir bar and thermometer. The resulting solution was stirred for 5 h at 80 ºC. The resulting solution was diluted with water (50 mL). The mixture was extracted with methyl tert-butyl ether (5 x 20 mL) and the organic layers were combined, dried over anhydrous sodium sulfate, filtered and concentrated under vacuum.

The residue was purified by column chromatography eluting with dichloromethane/methanol (50:1 v/v) to give *tert*-butyl 4-((1-(4-fluorophenyl)-4-oxo-1,4-dihydro-5*H*-pyrazolo[3,4-*d*]pyrimidin-5-yl)methyl)-4-hydroxypiperidine-1-carboxylate **(**500 mg, 26%). LCMS: (ESI) *m/z* 444 [M+H].

Step 5. **1-(4-Fluorophenyl)-5-((4-hydroxypiperidin-4-yl)methyl)-1,5-dihydro-4*H*-pyrazolo [3,4-*d*]pyrimidin-4-one trifluoroacetic acid salt**

tert-Butyl 4-((1-(4-fluorophenyl)-4-oxo-1,4-dihydro-5*H*-pyrazolo[3,4-*d*]pyrimidin-5-yl)methyl)-4-hydroxypiperidine-1-carboxylate (Step 4, 500 mg, 1.13 mmol), dichloromethane (30 mL) and trifluoroacetic acid (3 mL) were added to a 50-mL round-bottom flask fitted with a magnetic stir bar and condenser. The resulting solution was stirred for 2 h at 25 ºC. The resulting mixture was concentrated under vacuum to give 1-(4-fluorophenyl)-5-((4-hydroxypiperidin-4-yl)methyl)-1,5-dihydro-4*H*-pyrazolo[3,4-*d*]pyrimidin-4-one trifluoroacetic acid salt which was used in Step 6 without further purification. LCMS: (ESI) *m/z* 344 [M+H].

Step 6. **5-((1-(4,4-difluoro-3-(3-fluoro-1H-pyrazol-1-yl)butanoyl)-4-hydroxypiperidin-4-yl)methyl)-1-(4-fluorophenyl)-1,5-dihydro-4H-pyrazolo[3,4-d]pyrimidin-4-one (FT671)**

To a 250-mL round-bottom flask was added 4,4-difluoro-3-(5-fluoro-1*H*-pyrazol-1-yl) butanoic acid (2.0 g, 9.61 mmol), *N,N*-dimethylformamide (40 mL), *N*-(3-Dimethylaminopropyl)-*N*'-ethylcarbodiimide hydrochloride (2.4 g, 12.5 mmol), Hydroxybenzotriazole (1.7 g, 12.6 mmol), *N,N*-diethylisopropylamine (3.7 g, 28.6 mmol), 1-(4-fluorophenyl)-5-((4-hydroxypiperidin-4-yl)methyl)-1,5-dihydro-4*H*-pyrazolo[3,4-d]pyrimidin-4-one, trifluoroacetic acid salt (Step 5, 4.4 g, 9.6 mmol). The resulting solution was stirred for 1 h at 22 °C. The reaction was poured into 200 mL of water and the solution was extracted with 3 x100 mL of ethyl acetate. The organic layers were combined and dried over anhydrous sodium sulfate. The solids were removed by filtration and the solution was concentrated under vacuum. The residue was filtered initially with a silica gel column eluting with ethyl acetate/petroleum ether (7:10). The collected fractions were combined and concentrated under vacuum. The material was further purified by Flash-Prep-HPLC with the following conditions (IntelFlash-1): Reverse-phase column; mobile phase, water (NH_4HCO_3, 10mmol/L)/acetonitrile = 10% increasing to water (NH_4HCO_3, 10 mmol/L)/acetonitrile = 70% within 50 min; Detector, UV 254 nm. The collected fractions were concentrated under

vacuum to give 5-((1-(4,4-difluoro-3-(3-fluoro-1*H*-pyrazol-1-yl)butanoyl)-4-hydroxypiperidin-4-yl)methyl)-1-(4-fluorophenyl)-1,5-dihydro-4*H*-pyrazolo[3,4-d]pyrimidin-4-one (7 g, 91%).

High-resolution mass spectrometry (HRMS): ($C_{24}H_{23}F_4N_7O_3$ – expected $[M+H]^+$ 534.18768, observed $[M+H]^+$ 534.187770 (0.17 ppm). Agilent QTOF 6560 ESI+ mode. Column: Waters Acquity UPLC BEH C18, 1.7 um, 2.1 x 50 mm. Mobile phase A: 95% Water/5% Acetonitrile with 0.1% Formic Acid /Mobile phase B: 95% Acetonitrile/5% Water with 0.085% Formic Acid. Flow rate: 20 mL/min. Column temperature: 35 °C. Gradient: 5-100% B in 2.0 min, hold 100% to 2.2 min. LC Flow Rate: 0.6 mL/min. UV Wavelength: 220 nm (**Supplementary Figure 2f**).

^{1}H NMR: (300 MHz, DMSO-d_6) δ 8.47 – 8.30 (m, 2H), 8.08 (dd, *J* = 9.0, 4.8 Hz, 2H), 7.81 (q, *J* = 2.8 Hz, 1H), 7.44 (t, *J* = 8.8 Hz, 2H), 6.26 (td, *J* = 55.0, 3.6 Hz, 1H), 6.00-5.90 (m, 1H), 4.97 (s, 2H), 4.15 – 3.96 (m, 3H), 3.70 (d, *J* = 13.6 Hz, 1H), 3.30 – 3.16 (m, 2H), 2.91 (ddd, *J* = 16.7, 11.7, 4.2 Hz, 2H), 1.72 – 1.27 (m, 4H) ppm (**Supplementary Figure 2g**).

^{19}F NMR (376 MHz, DMSO-d_6) δ -131.12 (br s, 1 F) -127.80 - -126.20 (m, 1 F) -125.84 - -123.99 (m, 1 F) -114.84 (br d, J=2.63 Hz, 1 F) ppm (**Supplementary Figure 2h**).

^{13}C NMR (101 MHz, DMSO-d_6) δ 30.8, 34.4, 34.5, 35.1, 37.7, 53.5, 60.0, 69.5, 90.0, 107.1, 115.1, 116.7, 124.1, 134.9, 136.7, 151.5, 152.2, 152.8, 159.8, 162.2, 164.5, 166.4 ppm (**Supplementary Figure 2i**).

FT671 chiral purification: Preparative supercritical fluid column (SFC) chromatography, (R,R)-WHELK-O1-Kromasil, 5cm x 25cm (5μM; mobile phase, CO_2 (50%), isopropylalcohol:acetonitrile = 2:1(50%); detector: UV 220nm.
First eluting isomer (FT671): 5-([1-[(3*S*)-4,4-difluoro-3-(3-fluoro-1*H*-pyrazol-1-yl)butanoyl]-4-hydroxypiperidin-4-yl]methyl)-1-(4-fluorophenyl)-1*H*,4*H*,5*H*-pyrazolo[3,4-d]pyrimidin-4-one (retention time: 5.78 min) (3.0 g) (**Supplementary Figure 2j**).

Second eluting isomer: 5-([1-[(3*R*)-4,4-difluoro-3-(3-fluoro-1*H*-pyrazol-1-yl)butanoyl]-4-hydroxypiperidin-4-yl]methyl)-1-(4-fluorophenyl)-1*H*,4*H*,5*H*-pyrazolo[3,4-d]pyrimidin-4-one (retention time: 7.74 min) (3.1 g) (**Supplementary Figure 2k**).

Surface plasmon resonance (SPR)

Studies of binding kinetics were performed on a Biacore T200 (GE Healthcare). His-tagged $USP7_{CD}$ WT and mutant proteins, and His-tagged PH domain of Akt (non-DUB negative control) were immobilised in 10 mM HEPES pH 7.5, 150 mM NaCl, 2 mM $CaCl_2$, 1 mM β-mercaptoethanol, 5% (v/v) glycerol, 0.01% Triton-X 100 on a Biacore Series S NTA chip through N-terminal His tag capture, followed by amine-coupling with EDC/NHS/Ethanolamine as per manufacturer's instructions, aiming for an immobilisation level of 10,000 RU.

Compounds were tested in duplicate in two-fold dilution series in immobilisation buffer supplemented with 3% (v/v) DMSO, with a flow rate of 30 µl min^{-1}, a contact time of 60 s, and a dissociation time of 300 s. A solvent correction curve from 2.4-3.8 % (v/v) DMSO was included. Ubiquitin at 20 µM was injected between compounds as a positive control, and ten-point dilution curves of ubiquitin from 500 µM were included before and after the compounds to ensure surface integrity was retained throughout.

Analysis was performed using the Biacore Evaluation software version 3.0 using a kinetic fit and a 1:1 binding model with the R_{max} fit locally. Representative curves were exported and re-plotted in GraphPad Prism.

The fact that the irreversible compound FT827 displays reversible behaviour is consistent with its measured k_{inact} value (0.0003 s^{-1} corresponding to $t_{½}$ = 38.5 min) and the short association time (60 s = 0.026 x $t_{½}$), from which the percentage of complexes forming a covalent bond would be predicted to be $100 – (100/2^{0.026}) = 1.8$ %.

Circular Dichroism (CD)

Analysis was carried out at the University of Cambridge's Biophysics Facility, using an Aviv Model 410 Circular Dichroism Spectrometer. $USP7_{CD}$ WT, $USP7_{CD}$ F291N, $USP7_{CD}$ Q297A, and $USP7_{CD}$ Y465N were buffer exchanged into CD buffer (10 mM potassium phosphate pH 7.5, 100 mM potassium fluoride, 1 mM DTT) using a Zeba Spin column, before dilution to ~0.2 mg ml^{-1}. CD experiments were carried out at room temperature, reading at wavelengths from 250 nm to 189 nm in 1 nm steps, with an averaging time of 3 s, setting time of 0.33 s, and 3 scans per wavelength. Data from scans were averaged, buffer-subtracted and smoothed, and data exported to GraphPad Prism for analysis.

In vitro USP7 activity assay

Fluorescence intensity measurements were used to monitor the cleavage of a monoubiquitinated ubiquitin-rhodamine substrate[20]. All activity assays were performed in black 384 well ProxiPlates (PerkinElmer) in 20 mM Tris pH 8.0, 2 mM $CaCl_2$, 1 mM reduced glutathione, 0.01% (v/v) Triton X100, 0.01% (v/v) Prionex and an assay volume of 10 µL.

To determine compound IC_{50}s, compounds were diluted in 100% DMSO in three-fold 12-point dilution series from 100 µM. 100 nL of 100-fold concentrated solutions were dispensed into black 384-well Proxiplates (Perkin Elmer) using an Echo (Labcyte). 25 nM Ubiquitin-Rhodamine 110 (Boston Biochem), along with recombinant $USP7_{CD}$ (3 nM), or $USP7_{C\text{-}term}$ (30-125 pM, depending on batch activity) were added and the plates incubated at room temperature for 1 h. The reaction was terminated by adding 2.5 µL citric acid to a final concentration of 10 mM prior to measuring fluorescence intensity on a Pherastar (BMG Labtech) with a 485 nm excitation/520 nm emission optic module.

To determine K_M/k_{cat} values, recombinant $USP7_{CD}$ (3 nM), $USP7_{CD}$ F291N (0.2 nM), $USP7_{CD}$ Q297A (16 nM), or $USP7_{CD}$ Y465N (100 nM), were incubated at room temperature for 1 h with a two-fold 15-point dilution series of Ubiquitin-Rhodamine 110 (Boston Biochem) from a top concentration of 5 µM. Upon addition of the substrate, fluorescence intensity was monitored kinetically on a Pherastar (BMG Labtech) with a 485 nm excitation/520 nm emission optic module. RFU were converted to pmol ubiquitin-rhodamine converted. Pmol $protein^{-1}$ by assuming 100% substrate conversion at each ubiquitin-rhodamine concentration in the presence of excess enzyme. Converted data were plotted in Graphpad Prism and the initial rate was determined from the slop of a linear fit of the early part of the curve (over ~10 min). Initial rates were plotted against substrate conversion and fitted to a k_{cat} fit in Graphpad Prism.

k_{inact}/K_I determination

For the covalent compound FT827, a k_{inact}/K_I assay was carried out using 125 pM $USP7_{C\text{-}term}$ as described above. Upon addition of the substrate, fluorescence intensity was monitored

kinetically over 3 h. Analysis was performed in ActivityBase (ID Business Solutions Limited). Kinetic progress curves were fitted to equation $y = y_{max}(1-\exp(-k_{obs}.x))$ to determine k_{obs}. k_{obs} was then plotted against the inhibitor concentration and fitted to the equation $y = k_{inact}/(1+(K_I/x))$ to determine k_{inact} and K_I.

***In vitro* compound specificity panel**

DUBprofiler™ assays were performed by Ubiquigent Ltd. (Dundee, UK). FT671 was tested at 50 µM using 100 nM Ubiquitin-rhodamine 110 as the substrate. For most enzymes, K_M exceeds substrate concentration. For USP11, USP15, USP20, UCHL1, UCHL3 and OTUD3, the K_M was similar or lower than substrate concentration, and the potency of competitive inhibitors may be underestimated.

Linearity of enzyme activity through the assay incubation time was validated for each DUB enzyme by Ubiquigent Ltd. All assays were operating at <40% substrate conversion and data are reported as a percentage of the activity of the enzyme in the presence of the test compound relative to 'plus' (100% activity) and 'minus' (0% activity) DUB enzyme controls. Four 'plus' enzyme control wells and 'Product Modulator' control wells were run on each DUBprofiler™ assay plate. Eight 'minus' enzyme control wells were run on each DUBprofiler™ assay plate.

DUB profiling assays using ubiquitin-based active site directed probes

Molecular probes based on the ubiquitin scaffold were generated and used essentially as described[7,23] with some modifications. In brief, HA-tagged ubiquitin bromoethyl (HA-UbC2Br) was synthesised by expressing the fusion protein HA-Ub_{75}-Intein-chitin binding domain in *E. coli* BL21 strains[22]. Bacterial lysates were prepared, and the fusion protein purified over a chitin binding column (NEB labs, UK). HA-Ub_{75}-thioester was obtained by incubating column material with mercaptosulfonate sodium salt (MESNa) overnight at 37 ^{o}C. HA-Ub_{75}-thioester material was desalted against PBS using a PD10 column according to the manufacturer's instructions (GE Healthcare). 500 µl of 1-2 mg ml^{-1} of HA-Ub_{75}-thiolester was incubated with 0.2 mmol of bromo-ethylamine at pH 8-9 (adjusted by adding NaOH) for 20 min at room temperature, followed by a desalting step against phosphate buffer (pH 8) as described above. Ubiquitin probe material was concentrated using 3,000 MW filters (Sartorius) until a concentration of ~1 mg ml^{-1}, and kept as aliquots at -80°C until use.

DUB competition assays with cell extracts and with cells (*in situ*)

Human breast cancer MCF7 cells were cultured in DMEM medium supplemented with 10% FCS, 1% penicillin/streptomycin and 1% glutamine at 37 ^{o}C and 5% CO_2. Crude extracts were prepared as described previously using glass-bead lysis in 50 mM Tris pH 7.4, 5 mM $MgCl2{\cdot}6H_2O$, 0.5 mM EDTA, 250 mM sucrose and 1 mM DTT[7,23] . For experiments with crude cell extracts, 50 µg of MCF7 cell lysate was incubated with different concentrations of either FT671 or FT827 for 1 h at 37 ^{o}C, followed by addition of 1 µg HA-UbC2Br and incubation for 5 min at 37 ^{o}C. Incubation with Ub-probe was optimised to minimise replacement of non-covalent inhibitor FT671 by the covalent probe. Samples were subsequently boiled in reducing SDS-sample buffer, separated by SDS-PAGE and analysed by Western blotting using anti-HA (12CA5, Roche, #11583816001, 1:2000) or anti-USP7 (Enzo #PW0540, 1:1000) or anti-β-Actin (Abcam #ab8227, 1:2000) antibodies. $5x10^6$ intact MCF7 cells were incubated with different concentrations of inhibitors in cultured medium for 4 h at 37 ^{o}C, followed by glass-bead lysis, labelling with HA-UbC2Br probe and analysis by SDS-PAGE and Western blotting as described above.

Mass spectrometry based DUB inhibitor profiling assays

Ub-probe pulldown experiments in presence of different concentrations of the inhibitors FT671 and FT827 were performed essentially as described[7,23] with some modifications. In brief, immunoprecipitated material was subjected to in-solution trypsin digestion [44] and desalted using C18 SepPak cartridges (Waters) according to the manufacturer's instructions. Digested samples were analysed in triplicate by nano-UPLC-MS/MS using a Dionex Ultimate 3000 nano UPLC with EASY spray column (75 µm x 500 mm, 2 µm particle size, Thermo Scientific) with a 60 min gradient of 0.1 % (v/v) formic acid in 5% (v/v) DMSO to 0.1% (v/v) formic acid to 35% (v/v) acetonitrile in 5% (v/v) DMSO at a flow rate of ~250 nl/min (~600 bar/40 ^{o}C column temperature). MS data were acquired with an Orbitrap Q Exactive High Field (HF) instrument in which survey scans were acquired at a resolution of 60.000 @ 400 m/z and the 20 most abundant precursors were selected for CID fragmentation. From raw MS files, peak list files were generated with MSConvert (Proteowizard V3.0.5211) using the 200 most abundant peaks/spectra. The Mascot (V2.3, Matrix Science) search engine was used for protein identification at a false discovery rate of 1 %, mass deviation of 10 ppm for

MS1 and 0.06 Da (Q Exactive HF) for MS2 spectra, Cys carbamidylation as fixed modification, Met oxidation and Gln deamidation as variable modification. Searches were performed against the UniProtKB human sequence data base (retrieved 15.10.2014). Label-free quantitation was performed using MaxQuant Software (v1.5.2), and data were further analysed using GraphPad Prism software (v7.0) and Microsoft Excel. For the statistical analysis in **Fig. 1e** and **1f**, we applied two-way ANOVA tests including multiple comparison testing via the Dunnett method available through the GraphPad Prism software. P value style is GP: 0.1234 (ns), 0.0332 (*), 0.0021 (**), 0.0002 (***), <0.0001 (****)

Expression and purification of USP7$_{CD}$ for crystallography

GST-tagged USP7$_{CD}$ (residues 208-560) was cloned into the pGEX4T vector and expressed in *E. coli* Rosetta2 cells as described in[24]. Cells were grown in TB at 37 °C to an OD_{600} of 0.6, induced with 0.4 mM IPTG and incubated overnight at 18 °C.

The cell pellet was re-suspended in lysis buffer C (50 mM HEPES pH 7.5, 300 mM NaCl, 1 mM DTT, 5 mM benzamidine, 1 mM PMSF) and lysed using a Constant Systems Ltd cell disruptor. Insoluble material was removed by centrifugation and the supernatant was loaded onto a column packed with Glutathione Sepharose 4B beads (GE Healthcare) and washed with GST Buffer (50 mM HEPES pH 7.5, 150 mM NaCl, 1 mM DTT) until A_{280} reached baseline.

The GST tag was cleaved off-column using thrombin and removed by reapplying the sample onto the GSH column. USP7$_{CD}$ was then separated from thrombin using Benzamidine Sepharose beads (GE Healthcare), and purified further by gel filtration (Superdex 200, GE Healthcare in 50 mM HEPES pH 7.5, 150 mM NaCl, 1 mM DTT). Protein was concentrated to 17.5 mg ml^{-1}, aliquoted, flash-frozen in liquid N_2 and stored at -80 °C.

Crystallisation

USP7$_{CD}$-FT671 structure

USP7$_{CD}$ was crystallised from 25 % (w/v) polyethylene glycol (PEG) 1500, 100 mM MMT (DL-malic acid, MES monohydrate, Tris, pH 8.0) at 20 °C for 24 h in sitting-drop vapour diffusion experiments. A crystal was soaked in a solution containing 1.25 mM FT671, 30 % (v/v) PEG 400, 17.5 % (w/v) PEG 1500, 70 mM MMT pH 8.0 for 72 h and flash-cooled in liquid N_2.

USP7$_{CD}$-FT827 structure

$USP7_{CD}$ was crystallised from 20 % (w/v) PEG 3350, 100 mM Bis-Tris propane pH 7.5, 0.2 M sodium formate at 20 °C for 24 h in sitting-drop vapour diffusion experiments. A crystal was soaked in a solution containing 2 mM FT827, 30 % (v/v) PEG 400, 14 % (w/v) PEG 3350, 70 mM Bis-Tris propane pH 7.5, 140 mM sodium formate for 24 h and was flash-cooled in liquid N_2.

Data collection and refinement

Data for the USP7-FT671 and FT827 complex structures were collected at Diamond Light Source (Harwell, UK), beamline I03 and I04, respectively, at 100 K, and processed to 2.35 Å and 2.33 Å resolution, respectively, using Xia2[45]. Structures were solved by molecular replacement with PHASER[46] and human $USP7_{CD}$ (PDB 1NB8[24]) as the search model. The model was rebuilt using COOT[47] and refined using REFMAC5[48]. Data collection and refinement statistics are shown in **Extended Data Table 2**. Ramachandran statistics are as follows: USP7-FT671: 95.3% favoured / 4.2% allowed / 0.5% outliers and USP7~FT827: 94.8% favoured / 4.7 % allowed / 0.5 % outliers. Figures were generated with PyMol (www.pymol.org), and Molecular Operating Environment (MOE) (v. 2013.08, Montreal, Canada).

Cellular studies with USP7 inhibitors

MM.1S cells were acquired from ATCC (Manassas, VA, CRL-2974) and their identity was authenticated using STR analysis. HCT116 cells were acquired from ATCC (ATCC-CCL-247, October 2016). IMR-32 were acquired from Sigma (cat. number 86041809, January 2016). MCF7 were acquired from ATCC (HTB-22). U2OS were acquired from ATCC (HTB-96, authenticated in March 2017). HCT116, MCF7 and U2OS cells were authenticated frequently. Cell lines used in this study were verified to be mycoplasma negative before undertaking any experiments with them.

Knockdown studies and Western blotting

MM.1S cells (ATCC) were grown, in log phase, in RPMI-1640 supplemented with 10 % fetal bovine serum and antibiotic/antimycotic solution. FT671 was added to cells at a final

concentration of 10 µM for 0 h, 2 h, 4h, 8 h or 24 h, as indicated. Cells were harvested from both the liquid fraction and the adherent fraction by collecting, washing with chilled PBS and snap-freezing at -80°C.

Cell lysate was prepared for western blotting by lysing with RIPA lysis buffer (Boston Bioproducts), followed by separation by SDS-PAGE and transfer to PVDF membrane using the iBlot2 system (Life Technologies). Blots were probed with antibodies against MDM2 (TA590124, Origene), p53 (DO-1, Santa Cruz Biotechnology), p21 (12D1, Cell Signaling Technologies) and β-actin (13E5, Cell Signaling Technologies). Membranes were developed using Pierce ECL Western blotting substrate (Fisher) and imaged on the Amersham Bioluminescent Imager (GE Healthcare).

HCT116, U2OS and IMR-32 cells were cultured in DMEM medium with Glutamax supplemented with 10 % FBS, 1 % nonessential amino acids, and 1 % penicillin/streptomycin (Gibco). For cellular assays with compound, cells were treated with 0.1 µM, 1 µM, 3 µM and 10 µM FT671 or vehicle as indicated. For siRNA experiments, cells were transfected with non-targeting (NT1) or target specific siRNA oligos (Dharmacon On Target Plus oligos, Thermo Fisher Scientific, **Supplementary Table 3**) at 40 nM final concentration for 72 h using RNAiMAX (Invitrogen). Cells were lysed with RIPA buffer (10 mM Tris-HCl pH 7.5, 150 mM NaCl, 1 % (v/v) NP40, 0.1 % (v/v) SDS, 1 % (v/v) sodium deoxycholate) supplemented with mammalian protease inhibitor (Sigma) and phosphatase inhibitor cocktails (Roche). 20 µg of protein lysates were resolved by SDS-PAGE (Invitrogen 4-12 % NuPage or 10 % Biorad gels) and transferred to nitrocellulose (Amersham Protran, GE Healthcare). Membranes were probed with anti-p53 (DO1, Santa Cruz), anti-MDM2 (IF2, Calbiochem), anti-MDM2 (2A10 and 4B2, gifts from Ted Hupp, University of Edinburgh), anti-p21 (F-5, Santa Cruz), anti-USP7 (Abcam), anti-N-Myc (Cell Signaling), anti-DNMT1 (D63A6, XP® Rabbit mAb Cell Signaling #5032), anti-UHRF1 (H-8, Santa Cruz Biotechnology sc-373750), and anti-β-actin (Abcam). Visualisation and quantitation of western blots were carried out using an Odyssey infrared scanner (LI-COR Biosciences, Lincoln, NE).

Compound resistant cell lines

GFP-USP7 was subcloned from pEGFP-C-GW-USP7 into pCDNA5-FRT-TO (Invitrogen). The coding sequences for F291N and Q297A were subcloned from pETNHT_USP7 K208-E560 (F291N) and pETNHT_USP7 K208-E560 (Q297A) plasmids into pCDNA5-GFP-USP7.

HCT116 Flp-In TRex cells (gift from Stephen Taylor, University of Manchester) were cultured in DMEM with Glutamax supplemented with 10 % FBS, 1 % nonessential amino acids solution, 1 % penicillin/streptomycin, 10 µg/mL zeocin, and 4 µg/mL blasticidin (Invitrogen).

HCT116 Flip-In Trex cells were transfected with Lipofectamine LTX, with Plus Reagent (Invitrogen), with pOG44 and either pEF5-GFP, pCDNA5-GFP-USP7WT, pCDNA5-GFP-USP7F291N or pCDNA5-GFP-USP7Q297A. Two days after transfection, Hygromycin B (50 µg/mL, Invitrogen) was added and cells were kept under selection for 3 weeks.

Stably transfected HCT116 Flip-In Trex GFP, GFP-USP7WT, GFP-USP7F291N and GFP-USP7Q297A cells were incubated with 0.1 µg/mL Doxycycline for 3 h, and then treated with 1 µM and 3 µM of FT671 or vehicle for 4 h in presence of doxycycline. Cells were lysed with RIPA lysis buffer supplemented with mammalian protease inhibitor (Sigma) and phosphatase inhibitor cocktails (Roche). Protein lysates were resolved by SDS-PAGE (10 % gel, BioRad), transferred to nitrocellulose (Amersham Protran, GE Healthcare). Membranes were probed as indicated.

Quantitative PCR analysis

MM.1S or HCT116 cells (ATCC) were grown, in log phase, in RPMI-1640 supplemented with 10% fetal bovine serum and an antibiotic/antimycotic solution. FT671 was added to cells at a final concentration of 10 µM for 0, 2, 4 8 or 24 h, as indicated. Cells were harvested from both the liquid fraction and the adherent fraction by collecting, washing with chilled PBS and snap-freezing at -80°C.

RNA was harvested from cells using the RNeasy Kit (Qiagen) and quantitated by Nanodrop. Transcripts were amplified and quantitated using the TaqMan RNA-to-Ct 1-step kit (Life Technologies) with TaqMan Probe sets on the QuantStudio7 Flex (Life Technologies) according to the manufacturer's directions. TaqMan primer sets were used for the following genes, CDKN1A (Hs00355782_m1, Life Technologies), BBC3 (Hs00248075_m1), MDM2 (H200540450_s1), RPS27L (Hs00955038_g1), Myc (Hs00153408_m1), MCL1 (Hs01050896_m1), GAPDH (Hs0392907g1). Cycle number and fold-change were quantified using the software for the QuantStudio7 Flex and plotted in Prism 7.0.

Meso Scale Discovery MDM2 ubiquitination assay

MM.1S cells were plated in a 96-well format (26.7K cells / well) and treated at the same time with compound FT671 (final concentration 10 µM, 0.1% DMSO) and proteasome inhibitor MG132 (final concentration 25 µM) (AlfaAesar, cat #: J63250LB0) or 0.1% DMSO, and harvested at indicated time points. The commercially available Meso Scale Discovery assay kit for Ubiquitinated and Total MDM2 in whole cell lysate (MSD, cat #: K15168D) was used as according to the manufacturer instruction to lyse and process the cell pellets. Measured is the ratio of ubiquitinated versus non-ubiquitinated total MDM2. Raw data from a triplicate experiment was plotted with Graphpad Prism.

Cell viability studies

MM.1S were plated at starting density 3500 cells/well in 40 µl of RPMI-1640 (Corning) supplemented with 2 mM L-glutamine, 10 % fetal bovine serum (Corning), 1 % penicillin/streptomycin, and 10 mM HEPES, pH 7.4. Cells were plated in 384-well black plates (Corning 3712) and incubated at 37 °C, 5 % CO_2 in humidified atmosphere for 12 h before DMSO-solubilised FT671 was added using an ECHO 525 acoustic dispenser. The final DMSO concentration was 0.5 % (v/v). After compound addition, cells were incubated for 120 h at 37 °C, 5 % CO_2 in humidified atmosphere. Experiments were performed in triplicate, at the same time on different plates.

The viability assay was performed using CellTiter-Glo 2.0 (Promega) following manufacturer instructions. Luminescence was measured using an Envision plate reader (PerkinElmer) and normalised to the samples treated with 0.5 % (v/v) DMSO. The IC_{50} values were calculated using nonlinear regression algorithms in ActivityBase (ID Business Solutions Limited).

MM.1S xenograft studies

6 to 8-week-old female NOD SCID mice (Vital River Laboratory Animal Technology Co, Beijing, China) were irradiated (200 rads) with a Co60 irradiator source 24 h prior to subcutaneous inoculation of 5x106 MM.1S tumour cells in 1:1 mixture of RPMI-1640 and Matrigel. The efficacy study was initiated when tumours had reached an average volume of 159 mm^3. Mice received a lead-in dose of 25 mg kg^{-1} of FT671 24h prior to starting on the

dosing regimen of 100 or 200 mg kg^{-1} FT671 (QD, p.o. by oral gavage). 10% DMA/90% PEG400 served as a vehicle control (n=9 mice/group). For the statistical analysis of differences in tumour volumes between treatment groups, a 2-way ANOVA with repeated measures was performed followed by correction for multiple comparisons using statistical hypothesis testing (Tukey).

For the PK/PD study, a single administration of 200, 75 or 25 mg kg^{-1} FT671 was given p.o. by oral gavage when tumours had reached an average volume of 318 mm^3. 10 % DMA / 90 % PEG 400 served as a vehicle control (n=5 mice/group/time point). Tumour samples were harvested at 0.5 h, 2 h, 6 h and 24 h time points and flash frozen for subsequent analysis. Vehicle control samples were harvested at 24 h time point.

For xenograft tumour tissue -analysis, flash frozen tissue samples were lysed in Tris Lysis buffer (Meso Scale Discovery, Rockville, MD) complemented with protease and phosphatase inhibitors (Roche, Mannheim, Germany). p53 levels were analysed from 20 μg of protein/sample by western blotting with anti-p53-antibodies (Santa Cruz sc-126, 1:200), anti-p21 (Cell Signaling Technology #4970, 1:1000). β-Actin (Cell Signaling Technology #2946, 1:1000) was used to normalise p53-levels. Secondary antibodies were HRP-conjugated anti-rabbit (Cell Signaling Technology #7074, 1:1000) and anti-mouse (Cell Signaling Technology #7076, 1:1000). ECL chemiluminescence detection reagents were used for detection and target bands were analysed using FluoChem FC2 software.

Animal experiments

All animal experiments were performed at Pharmaron (Beijing, China). All the animal experiments were performed according to the guidelines approved by the Institutional Animal Care and Use Committee (IACUC) of Pharmaron (Beijing, China) following the guidance of the Association for Assessment and Accreditation of Laboratory Animal Care (AAALAC). The protocol defines 3000 mm^3 as the maximum tumour volume for a humane endpoint and animals with larger tumours were euthanised.

Data availability

FT671 and FT827 are available from FORMA Therapeutics. All reagents are available by reasonable requests to the corresponding authors. Crystallographic coordinates and structure factors have been deposited with the Protein Data Bank under accession codes 5NGE (USP7-FT671) and 5NGF (USP7~FT827). MS data are available via ProteomeXchange with identifier PXD006418 and can also be found in **Supplementary Tables 1 and 2**. Uncropped images of all gels and blots in this study can be found in **Supplementary Figure 1**. Chemical characterisation of FT671 and FT827 can be found in **Supplementary Figure 2**. Source data are provided for animal experiments (**Fig. 5b-d, Extended Data Fig. 8e**) as well as for biophysical compound characterization and biological experiments.

Methods References

44. Fischer, R. & Kessler, B. M. Gel-aided sample preparation (GASP)--a simplified method for gel-assisted proteomic sample generation from protein extracts and intact cells. *Proteomics* **15,** 1224–1229 (2015).
45. Waterman, D. G. *et al.* Diffraction-geometry refinement in the DIALS framework. *Acta Crystallogr D Struct Biol* **72,** 558–575 (2016).
46. McCoy, A. J. *et al.* Phaser crystallographic software. *J Appl Crystallogr* **40,** 658–674 (2007).
47. Emsley, P., Lohkamp, B., Scott, W. G. & Cowtan, K. Features and development of Coot. *Acta Crystallogr D Biol Crystallogr* **66,** 486–501 (2010).
48. Murshudov, G. N. *et al.* REFMAC5 for the refinement of macromolecular crystal structures. *Acta Crystallogr D Biol Crystallogr* **67,** 355–367 (2011).

Extended Data Figure 1. Compound characterisation.

a, Schematic diagram of the USP7 constructs used in this study. **b**, Representative SPR sensorgrams of $USP7_{CD}$ and Akt Pleckstrin homology (PH) domain (negative control) to measure affinity parameters (K_d) of FT671 and FT827. Compounds were tested in 2-fold dilutions from 50 µM (FT827) or 1.56 µM (FT671). Sensorgrams are plotted showing two technical replicates. These data are representative of three biological replicates. Errors represent standard deviation of the mean. **c,** IC_{50} curves for FT671 against $USP7_{C\text{-}term}$ (Δ) and $USP7_{CD}$ (■) in the ubiquitin-rhodamine assay. The graph displays three biological replicates, each point representing the average of three technical replicates. **d,** Time course of the inhibition of $USP7_{C\text{-}term}$ by the covalent inhibitor FT827 used to derive k_{obs} values at each concentration. k_{obs} plot for covalent inhibitor FT827 used to derive the kinetic parameters. 18 biological replicates were run in singlicate, a representative singlicate is shown. See **Online Methods** for a detailed description of the synthesis and **Supplementary Figure 2** for the characterisation of the inhibitor compounds.

Extended Data Figure 2. USP7 target engagement and specificity in MCF7 cells.

a, Schematic representation of DUB activity-based profiling of small molecule inhibitors. Compounds were incubated either with intact MCF7 cells (*in situ*) or crude cell extracts, followed by labelling with the active site DUB probe HA-UbC2Br. DUBs either targeted by compounds or labelled by the DUB probe were visualised either by Western blotting or subjected to immunoprecipitation for enrichment and analysis by quantitative mass spectrometry [7,23]. **b-e**, FT671 and FT827 selectively target USP7 and disallow HA-UbC2Br binding, but do not notably interact with other DUBs as assessed by anti-HA immunoblotting. One out of two independent biological replicates is shown. **b**, MCF7 cell extracts incubated with FT617, **c**, intact MCF7 cells incubated with FT671, **d**, MCF7 cell extracts incubated with FT827, **e**, intact MCF7 cells incubated with FT827. **f,** Immunoprecipitation of cellular DUBs captured by HA-UbC2Br labelling for 10 min after incubation of MCF7 cell extracts with DMSO, 1 µM or 10 µM of FT671, FT827 or 50 µM P22077 for 60 min. Immunoprecipitated material was separated by SDS-PAGE and analysed by Western blotting using the indicated antibodies. **g**, FT671, FT827 and P22077 were incubated with MCF7 cell extracts at the indicated concentrations for 60 min, followed by labelling with HA-UbC2Br for either 5 min (*left*) or 60 min (*right*). Immunoprecipitated material was separated by SDS-PAGE and analysed by Western blotting using the indicated antibodies. Uncropped images for gels are shown in **Supplementary Figure 1.**

.

Extended Data Figure 3. Electron density for FT827 and FT671.

Stereo representation of $2|F_o|-|F_c|$ electron density maps, contoured at 1 σ, covering all atoms of the inhibitors in each of the two independent USP7 molecules of the asymmetric unit. Protein is shown as in **Fig. 2a**, and compound carbon atoms are in yellow. **a**, FT671; **b**, FT827; **c**, FT827 in an orientation to show the covalent linkage between inhibitor and Cys223.

Extended Data Figure 4. Schematic of FT671 and FT827 interactions with USP7.
Compound interactions and surrounding residues are labelled, hydrogen bonds indicated, and residues shown according to their chemical properties (see legend). The images were generated with Molecular Operating Environment (MOE) (v. 2013.08, Montreal, Canada). **a**, FT671; **b**, FT827.

Extended Data Figure 5. Molecular basis for USP7 compound specificity.

a, Superposition of USP7-FT671 complex with indicated DUBs. Shown are the isolated cartoon structures superimposed in **Fig. 3a** and **3b**. USP7 apo and USP7-FT671 (*top left*) show an identical switching loop position, whereas the corresponding region in other apo USP structures is in a distinct conformation that resembles the USP7~Ub complex (see **Fig. 3a, b**). Structures displayed: USP7 apo, PDB 1NB8 [24]; USP4 apo, PDB 2Y6E [40]; USP8 apo, PDB 2GFO [41]; USP12 apo, PDB 5K16 [42]; USP14 apo, PDB 2AYN [43]. **b**, Binding site detail, showing the interactions between Palm domain Tyr residues (Tyr465 and Tyr514 in USP7) and the Thumb domain and switching loop backbone present in all USP apo structures. The USP7 apo switching loop conformation disallows the Tyr465 interaction, which rotates away from the Thumb domain, and allows Tyr514 to adopt a buried conformation (Tyr514 'down' position). This generates space for compound binding. In other USP apo structures, the equivalent Tyr residues form hydrogen bonds with the switching loop and occupy the compound binding site.

Extended Data Figure 6. Characterisation of compound resistant USP7 mutants.

a-c, SPR based binding of FT671 (**a**), FT827 (**b**) and ubiquitin (**c**) to indicated USP7 mutants. For compound binding to wild-type $USP7_{CD}$ and Akt-PH controls, see **Extended Data Fig. 1b**. Sensorgrams are plotted showing two technical replicates. These data are representative of three biological replicates. Error range in **c** represents standard deviation of the mean. **d**, Summary table of binding constants observed for experiments in **Extended Data Fig. 1b** and **6a-c**. Biological repeats are indicated (n=9 for $USP7_{CD}$ WT, n=3 for $USP7_{CD}$ mutants), and errors indicate the standard error of the mean range observed. **e**, Circular dichroism profiles of $USP7_{CD}$ WT (red), $USP7_{CD}$ F291N (orange), $USP7_{CD}$ Q297A (green), and $USP7_{CD}$ Y465N (blue); each experiment was performed in triplicate. **f,** Tabulated values for experiments shown in **Fig. 3f**. SEM, standard error of the mean. **g,** Structure of activated USP7. The switching loop in USP7 is a point of intrinsic allosteric regulation, provided by a C-terminal module of five ubiquitin-like domains (termed HUBL1 to HUBL5) followed by an activation peptide (aa 1084-1102)[26] (see **Extended Data Fig. 1a**). In full-length USP7, the activation peptide stabilises the active conformation of the switching loop in the ubiquitin bound state[26-28], and this can be modulated by USP7 activating proteins such as GMPS[26,29]. Shown is the structure of activated USP7 bound to its C-terminal activation peptide. The model was generated from PDB 5JTV [27], and shown are the catalytic domain with ubiquitin in the S1 site (coloured as in **Fig. 2a**) of molecule 1 in the asymmetric unit, and the HUBL5 domain and activation peptide (orange) of molecule 2 in the asymmetric unit, which in the crystal binds to molecule 1 *in trans*. Uncropped images for gels are shown in **Supplementary Figure 1.**

Extended Data Figure 7. USP7 knockdown or inhibitors affect USP7 substrates in cell lines. **a**, HCT116 cells were transfected with non-targeting control (NT1) or three different USP7-targeting siRNAs for 72 h, harvested and probed with indicated antibodies. A representative experiment from two biological replicates is shown. **b**, U2OS cells transfected with a pool of 4 independent siRNAs targeting USP7 or a non-targeting control siRNA, as in **a**. A representative experiment from two biological replicates is shown. **c**, HCT116 cells were treated with 10 μM FT671 for 24 h and RNA was extracted for real-time PCR measurements with primer sets against indicated transcripts (see **Methods**). Data were analysed with the delta-CT method. Experiments were performed in triplicate. **d**, HCT116 cells were treated with FT671 (10 μM) for indicated, longer periods, harvested and probed with indicated antibodies. A representative experiment from two biological replicates is shown. **e,** Experiment as in **Fig. 4d**, with higher FT671 concentration. p53 levels are upregulated upon FT671 treatment in cells expressing USP7 WT, but not in cells expressing compound resistant mutants. USP7 expression was induced for 7 h by 1 μg/mL doxycycline, and cells were treated for 4 h with 3 μM FT671. **f**, IMR-32 neuroblastoma cells[33] were treated with indicated concentrations of FT671, and effects on p53 and N-Myc levels were tested by Western blotting. A representative experiment from two biological replicates is shown. **g, h,** HCT116 (**g**) or MM.1S (**h**) cells were treated for indicated times with FT671, and Western blotted for UHRF1 and DNMT1. Vinculin and actin serve as loading controls. A representative experiment from two biological replicates is shown. Uncropped images for gels are shown in **Supplementary Figure 1.**

Extended Data Figure 8. Characterisation of FT671 effects *in vivo*.

a, MM.1S cells were treated for the indicated times with 10 μM FT671, and proteins detected by Western blotting with indicated antibodies (see **Methods**). A representative experiment from two biological replicates is shown. **b,** Meso Scale analysis (see **Methods**) measuring the ratio of ubiquitinated versus non-ubiquitinated MDM2 in MM.1S cells upon FT671 treatment and proteasome inhibition (25 μM MG132). **c**, MM.1S cells were treated with 10 μM FT671 for the indicated times and RNA was extracted for real-time PCR measurements with primer sets against indicated transcripts (see **Methods**). Data were analysed with the delta-CT method. Experiments were performed in duplicate. **d,** qPCR analysis as in **c** using a single time point against *MCL1* and *c-Myc*, which in this setting are not p53 target genes after 24 h of 10 μM FT671. Experiments were performed in triplicate. **e**, MM.1S tumour xenograft tissues were analysed for p53 expression by Western blotting and normalised for β-actin loading control. Uncropped images for gels are shown in **Supplementary Figure 1.**

Extended Data Table 1. FT671 and FT827 specificity.

Tabulated specificity data of FT671 and FT827 at 50 μM against a panel of named DUBs of different families, graphically depicted in **Fig. 1b**. (1) +Ubiquitin@K_d; (2) +Ubiquitin@B_{max}; (3) Proteasome-VS@K_d; (4) USP10 and USP47 were tested individually at 25 μM FT671; N.D. , not determined.

Extended Data Table 2. Data collection and refinement statistics.

Values in parentheses are for the highest resolution shell. All datasets were collected from a single crystal each.